(12)

RADIOSCIENCE LABORATORY

STANFORD ELECTRONICS LABORATORIES
DEPARTMENT OF ELECTRICAL ENGINEERING
STANFORD UNIVERSITY · STANFORD, CA 94305

ULF/ELF ELECTROMAGNETIC FIELDS PRODUCED IN SEA WATER BY LINEAR CURRENT SOURCES

by

A.S. Inan
A.C. Fraser-Smith
O.G. Villard, Jr.

Technical Report E721-1

February 1982

Sponsored by
The Office of Naval Research
through
Contract No. N00014-79-C-0848

PAGES _____

ARE

MISSING

IN

ORIGINAL

DOCUMENT

UNCLASSIFIED

SECURITY CLASSIFICATION OF THIS PAGE (When Data Entered)

REPORT DOCUMENTATION PAGE		READ INSTRUCTIONS BEFORE COMPLETING FORM
1 REPORT NUMBER Technical Report No. E721-1	2. GOVT ACCESSION NO. AD-A119341	3. RECIPIENT'S CATALOG NUMBER
4. TITLE (and Subtitle) ULF/ELF Electromagnetic Fields Produced in Sea Water by Linear Current Sources		5. TYPE OF REPORT & PERIOD COVERED Technical 15 August 1979-31 January 1982
		6. PERFORMING ORG. REPORT NUMBER E721-1
7. AUTHOR(s) A. S. Inan A. C. Fraser-Smith O. G. Villard, Jr.		8 CONTRACT OR GRANT NUMBER(s) N00014-79-C-0848
9 PERFORMING ORGANIZATION NAME AND ADDRESS Radioscience Laboratory Stanford Electronics Lab., Stanford University Stanford, California 94305		10. PROGRAM ELEMENT, PROJECT, TASK AREA & WORK UNIT NUMBERS Task Area NR 089-151
11 CONTROLLING OFFICE NAME AND ADDRESS Office of Naval Research, Code 414 800 North Quincy Street Arlington, VA 22217		12. REPORT DATE February 1982 13. NO. OF PAGES 118
14 MONITORING AGENCY NAME & ADDRESS (if diff. from Controlling Office)		15. SECURITY CLASS. (of this report) UNCLASSIFIED
		15a. DECLASSIFICATION/DOWNGRADING SCHEDULE

16. DISTRIBUTION STATEMENT (of this report)

Approved for public release; distribution unlimited.

17 DISTRIBUTION STATEMENT (of the abstract entered in Block 20, if different from report)

18 SUPPLEMENTARY NOTES

19 KEY WORDS (Continue on reverse side if necessary and identify by block number)

UNDERSEA COMMUNICATION
SUBMERGED CABLES
ULF/ELF
"LEADER GEAR"
POINT ELECTRODES

20 ABSTRACT (Continue on reverse side if necessary and identify by block number)

This report is concerned with the possibility of using undersea cables to communicate with undersea receivers at frequencies in the ultra low and extremely low ranges. Because of the low data transmission rate at these frequencies, communication is here understood to mean the transfer of short messages of high information content.

We start by deriving theoretical expressions for the electric and magnetic fields generated in conducting medium of infinite extent by linear current

DD FORM 1 JAN 73 1473

EDITION OF 1 NOV 65 IS OBSOLETE

UNCLASSIFIED

SECURITY CLASSIFICATION OF THIS PAGE (When Data Entered)

19 KEY WORDS (Continued)

20 ABSTRACT (Continued)

sources (i.e., straight insulated current-carrying cables) of finite and semi-infinite length and of finite length with gaps of either finite or infinitesimal size. Next, using numerical integration techniques and, in some cases, a parametric representation to make our results frequency independent, we compute representative numerical values of the field amplitudes for the above discontinuous sources. For comparison with these data, we compute an extensive range of field amplitudes for the more frequently encountered continuous linear source of infinite length (i.e., a very-long straight insulated current-carrying cable); we also introduce a parametric representation for the fields produced by this reference source and we show that for any fixed perpendicular distance from the source there is an optimum frequency for electric field generation.

We show that the discontinuous sources generally produce greatly enhanced electric fields in the vicinity of their open ends, as compared with the continuous source. However, at large distances none of the discontinuous sources we have considered produce larger fields than the continuous source, and in most cases the discontinuous sources produce smaller fields. These results suggest that the optimum use of the discontinuous sources (short lengths of current-carrying cables; point electrodes) is for short-range undersea communication, whereas long continuous current-carrying cables appear to have the most promise for long-range communication via their electric and magnetic fields.

Finally, because even long cables have limited communication ranges at all but the lowest ultra low frequencies, we consider the use of arrays of parallel long cables to produce measurable electric and magnetic fields throughout specific regions of the sea. Our data indicate, for example, that a series connected array of 10 long cables (each of length L) laid on the floor of a sea 1 km deep and carrying a 1000 A, 1 Hz current could produce measurable magnetic fields throughout the sea over a horizontal area of about 75L km^2. Such arrays could find use in crucial areas where reliable undersea communication is of high priority.

ULF/ELF ELECTROMAGNETIC FIELDS PRODUCED IN SEA WATER BY LINEAR CURRENT SOURCES

by

A. S. Inan

A. C. Fraser-Smith

O. G. Villard, Jr.

Technical Report E721-1

February 1982

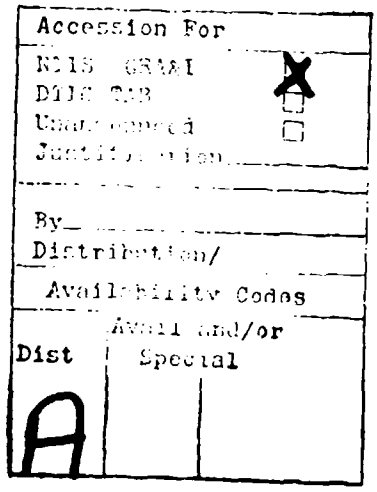

Sponsored by

The Office of Naval Research

through

Contract No. N00014-79-C-0848

ABSTRACT

This report is concerned with the possibility of using undersea cables to communicate with undersea receivers at frequencies in the ultra low and extremely low ranges. Because of the low data transmission rate at these frequencies, communication is here understood to mean the transfer of short messages of high information content.

We start by deriving theoretical expressions for the electric and magnetic fields generated in a conducting medium of infinite extent by linear current sources (i.e., straight insulated current-carrying cables) of finite and semi-infinite length and of infinite length with gaps of either finite or infinitesimal size. Next, using numerical integration techniques and, in some cases, a parametric representation to make our results frequency independent, we compute representative numerical values of the field amplitudes for the above discontinuous sources. For comparison with these data, we compute an extensive range of field amplitudes for the more frequently encountered continuous linear source of infinite length (i.e., a very-long straight insulated current-carrying cable); we also introduce a parametric representation for the fields produced by this reference source and we show that for any fixed perpendicular distance from the source there is an optimum frequency for electric field generation.

We show that the discontinuous sources generally produce greatly enhanced electric fields in the vicinity of their open ends, as compared with the continuous source. However, at large distances none of the discontinuous sources we have considered produce larger fields

than the continuous source, and in most cases the discontinuous sources produce smaller fields. These results suggest that the optimum use of the discontinuous sources (short lengths of current-carrying cable; point electrodes) is for short-range undersea communication, whereas long continuous current-carrying cables appear to have the most promise for long-range communication via their electric and magnetic fields.

Finally, because even long cables have limited communication ranges at all but the lowest ultra low frequencies, we consider the use of arrays of parallel long cables to produce measurable electric and magnetic fields throughout specific regions of the sea. Our data indicate, for example, that a series connected array of 10 long cables (each of length L) laid on the floor of a sea 1 km deep and carrying a 1000 A, 1 Hz current could produce measurable magnetic fields throughout the sea over a horizontal area of about 75L km^2. Such arrays could find use in crucial areas where reliable undersea communication is of high priority.

ACKNOWLEDGEMENT

Support for this work was provided by the Office of Naval Research through Contract No. N00014-79-C-0848.

Note: In this report we use the abbreviation ULF (ultra-low-frequencies) for frequencies less than 5 Hz, and we use ELF (extremely-low-frequencies) to designate frequencies in the range 5 Hz to 3 kHz.

TABLE OF CONTENTS

I. INTRODUCTION

Shortly after the end of the First World War a pair of articles appeared in the scientific literature describing experiments and theoretical work on the electromagnetic fields produced in, on, and above the sea by submerged cables carrying alternating current [Drysdale, 1924; Butterworth, 1924]. As described in the article by Drysdale [1924], and in greater detail in a later article by Wright [1953], this work was undertaken as part of a British Navy project called "Leader Gear", which was concerned with the use of the cable-generated electromagnetic fields for navigation. No further articles appeared on the fields produced by submerged cables until after the end of the Second World War, when Von Aulock prepared two lengthy unpublished reports on the subject [Von Aulock, 1948, 1953]. With the exception of a useful summary of Von Aulock's results by Kraichman [1976] and several particularly pertinent articles by Wait [1952, 1959, 1960], little research has since been carried out on the electromagnetic fields produced by submerged cables. This is unfortunate, because it is our belief that the fields could have important applications in undersea communication. The primary objective of this report is to take the work just described through a further stage of development and thus provide an improved theoretical basis for studies of the feasibility of the use of the fields from submerged cables for undersea communication.

To achieve this objective, we start with the comparatively well-known expressions for the electromagnetic fields produced in a conducting medium of infinite extent by a current element and then, always

considering a conducting medium of infinite extent, to systematically derive the other known expressions for (1) the electric field produced by a linear current source of finite extent (i.e., by a short current-carrying insulated wire or cable) and (2) the electric and magnetic fields produced by a linear current source of infinite length (i.e., by a long current-carrying insulated wire or cable). In passing we derive (3) an expression for the magnetic field produced by the linear current source of finite extent, which is a new result, and we solve this expression numerically to provide illustrative magnetic field data. We then expand from this beginning by deriving (4) expressions for the electric and magnetic fields produced by a linear current source of semi-infinite extent, with particular emphasis on the fields produced around the end of the source where the current enters the conducting medium. These latter results are then used to give (5) expressions for the electric and magnetic fields produced by two aligned, separated semi-infinite linear current sources, i.e., the fields produced in the vicinity of two point electrodes immersed in the conducting medium. Finally, we allow the spacing between the ends of linear sources in (5) to become infinitesimal and thus obtain (6) expressions for the electric and magnetic fields produced by a linear current source of infinite extent containing an infinitesimal gap. As we will show, these latter expressions can also be derived by subtracting the electric and magnetic field expressions for a current element from the equivalent expressions for a linear current source of infinite length.

In cases (4) to (6) above we present representative numerical

values for the electric and magnetic fields that are produced. We believe both these numerical values and the theoretical expressions for the electromagnetic fields are new. We end with a brief discussion of the possible application of the electric and magnetic fields to undersea communication.

There is one technical feature of our theoretical approach that has general implications and which is best discussed at this introductory stage. It will be noted that we always assume an infinitely thin cross-section for the various (cylindrical) linear current sources considered in this work, whereas it is obvious that these sources will have a finite cross-section in practice. Technically, this assumption takes the form of a replacement of a volume integral in the Hertz vector expression by an approximate line integral. The derivation of the approximate line integral is given in Appendix A and it is shown that the approximation is valid provided the shortest distance from the observation point to the surface of the current source is much greater than the radius of the source. Provided this condition is met, our expressions should give accurate values for the electric and magnetic fields produced by the linear current sources of finite cross-section.

The most important quantity to keep in mind in this work is the skin depth δ defined by

$$\delta = (2/\omega\mu\sigma)^{\frac{1}{2}} \qquad (I.1)$$

for a magnetic ($\mu \neq \mu_0$) conducting medium, where we use ω for the angular frequency, μ for the permeability of the medium (μ_0 is the permeability of free space), and σ for its conductivity. At the frequencies

considered in this report, electromagnetic fields propagate in a conducting medium with a wavelength given by $\lambda = 2\pi\delta$, and evidence of this wavelength will be seen in most of the figures showing numerical data. In all cases these numerical data are computed for sea water, where we assume $\sigma = 4.0$ S/m and $\mu = \mu_0 = 4\pi \times 10^{-7}$ H/m. Table I.1 lists numerical values of skin depth for these assumed sea water parameters and for frequencies in the range 0.001 - 1000 Hz.

The theory developed in this report assumes that the contribution from the displacement current term in Maxwell's equations can be neglected in comparison with the contribution from the conduction current term. This is only possible for frequencies satisfying the condition $\sigma/\omega\varepsilon >> 1$, where ε is the permittivity of the medium. In the case of sea water, which is the conducting medium of primary interest in this work, the above condition implies that the frequencies must be very much less than 890 MHz for our field expressions to be valid. This means that the frequencies must be below the microwave range (the lowest microwave frequency is usually taken to be 300 MHz) or, perhaps more strictly, they must be less than 100 MHz.

For frequencies satisfying the condition $\sigma/\omega\varepsilon >> 1$ (i.e., for frequencies less than 100 MHz in sea water) it is easily shown that electric fields propagating in a conducting medium are attenuated at the rate of 55 db/wavelength. This is a very substantial rate of attenuation and it is obvious as a result that large ranges for communication through sea water by means of electromagnetic signals can only be achieved by using low frequencies. It is for this reason that we have

Table I.1 Representative Skin Depths for Sea Water

(σ_s = 4.0 S/m)

Frequency (Hz)	Skin Depth (m)	Frequency (Hz)	Skin Depth (m)
1000	8.0	1	251.6
800	8.9	0.8	281.3
600	10.3	0.6	324.9
600	12.6	0.4	397.9
200	17.8	0.2	562.7
100	25.2	0.1	795.8
80	28.1	0.08	889.7
60	32.5	0.06	1027.3
40	39.8	0.04	1258.2
20	56.3	0.02	1779.4
10	79.6	0.01	2516.5
8	89.0	0.008	2813.5
6	102.7	0.006	3248.7
4	125.8	0.004	3978.9
2	177.9	0.002	5627.0
1	251.6	0.001	7957.7

restricted our computations of numerical data to frequencies in the extremely-low (ELF; frequencies in the range 5 Hz - 3 kHz) and ultra-low (ULF; frequencies less than 5 Hz) frequency bands. At these low frequencies the wavelength in sea water becomes usefully large (1.58 km at 1 Hz) and reasonably large communication ranges become possible. However, even at these low frequencies the same basic attenuation rate of 55 db/wavelength still applies and evidence for it will be found in all of our numerical data.

II. CURRENT ELEMENT SOURCE

Suppose we have a homogeneous isotropic conducting medium of conductivity σ, dielectric constant ϵ, and permeability μ. Assuming that all the fields vary with time t as $\exp(i\omega t)$, Maxwell's equations can be written in the form

$$\text{div } \underset{\sim}{E} = 0 \tag{II.1}$$

$$\text{div } \underset{\sim}{H} = 0 \tag{II.2}$$

$$\text{curl } \underset{\sim}{E} = -i\omega\mu \underset{\sim}{H} \tag{II.3}$$

$$\text{curl } \underset{\sim}{H} = (\sigma + i\omega\epsilon)\underset{\sim}{E} + \underset{\sim}{J} \tag{II.4}$$

where $\underset{\sim}{J}$ is the impressed current density and where $\underset{\sim}{E}$ and $\underset{\sim}{H}$ are the electric and magnetic field intensities, respectively. We wish to obtain $\underset{\sim}{E}$ and $\underset{\sim}{H}$ for a current element $Id\ell$ immersed in this conducting medium, which we will assume is of infinite extent.

In our derivation, and throughout this report, we will make extensive use of the Hertz vector $\underset{\sim}{\Pi}$ [Panofsky and Phillips, 1962; Kraichman, 1976], from which the $\underset{\sim}{E}$ and $\underset{\sim}{H}$ fields can be obtained by using the following equations in conjunction with Maxwell's equations II.1 - II.4:

$$\underset{\sim}{E} = -\gamma^2 \underset{\sim}{\Pi} + \text{grad div } \underset{\sim}{\Pi}, \tag{II.5}$$

$$\underset{\sim}{H} = \frac{\gamma^2}{i\omega\mu} \text{ curl } \underset{\sim}{\Pi}. \tag{II.6}$$

Here, γ, the propagation constant, is defined by

$$\gamma = \left(i\omega\mu(\sigma + i\omega\epsilon)\right)^{1/2}. \tag{II.7}$$

Substitution of Equations (II.5) and (II.6) into either (II.3) or (II.4) yields the differential equation

$$\text{curl curl } \underset{\sim}{\Pi} - \text{grad div } \underset{\sim}{\Pi} + \gamma^2 \underset{\sim}{\Pi} = \frac{\underset{\sim}{J}}{\sigma + i\omega\varepsilon} \quad , \tag{II.8}$$

which can also be written as

$$(\nabla^2 - \gamma^2)\underset{\sim}{\Pi} = \frac{-\underset{\sim}{J}}{\sigma + i\omega\varepsilon} \quad . \tag{II.9}$$

This equation is called the inhomogeneous wave equation and for our unbounded conducting medium it has a solution of the form (e.g., Wait, 1959)

$$\underset{\sim}{\Pi} = \frac{1}{4\pi(\sigma + i\omega\varepsilon)} \int_V \frac{e^{-\gamma r}}{r} \underset{\sim}{J} \, dv. \tag{II.10}$$

For a current element source oriented in the z-direction in a cylindrical coordinate system, as shown in Figure II.1, one can easily verify that the Hertz vector at the point P has only a z-component given by

$$\Pi_z(\rho,z) = \frac{Id\ell}{4\pi(\sigma + i\omega\varepsilon)} \frac{e^{-\gamma r}}{r} \quad , \tag{II.11}$$

where

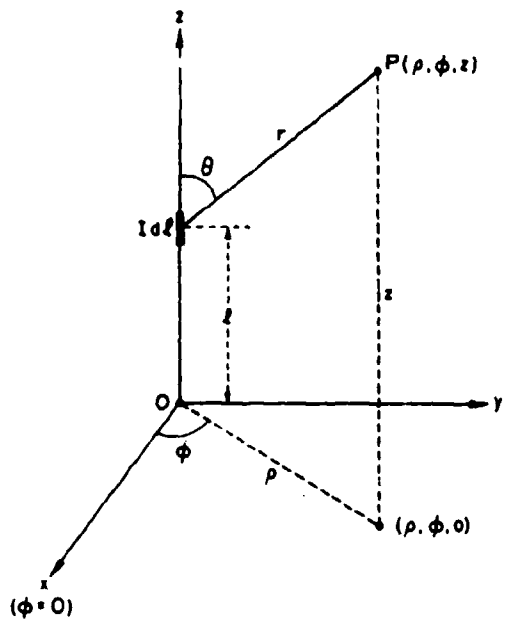

Figure II.1. Coordinate system and geometry used in the derivation of the electric and magnetic fields produced in a conducting medium of infinite extent by a current element Idℓ.

$$r = \left(\rho^2 + (z-\ell)^2 \right)^{\frac{1}{2}} .$$

Using this component of $\underset{\sim}{\Pi}$, the electric and magnetic fields can be obtained by performing the operations

$$\left.\begin{aligned} E_\rho &= \frac{\partial^2 \Pi_z}{\partial \rho \partial z} , \\ E_\phi &= 0 , \\ E_z &= -\gamma^2 \Pi_z + \frac{\partial^2 \Pi_z}{\partial z^2} , \end{aligned}\right\} \qquad \text{(II.12)}$$

and

$$\left.\begin{aligned} H_\rho &= 0 , \\ H_\phi &= \frac{-\gamma^2}{i\omega\mu} \frac{\partial \Pi_z}{\partial \rho} , \\ H_z &= 0 . \end{aligned}\right\} \qquad \text{(II.13)}$$

It follows from these equations that

$$\left.\begin{aligned} E_\rho &= \frac{Id\ell \sin\theta\cos\theta}{4\pi(\sigma+i\omega\varepsilon)r^3} \left(\gamma^2 r^2 + 3\gamma r + 3\right) e^{-\gamma r} , \\ E_\phi &= 0 , \end{aligned}\right\} \qquad \text{(II.14)}$$

$$E_z = \frac{Id\ell}{4\pi(\sigma+i\omega\varepsilon)r^3}\left[\cos^2\theta(\gamma^2r^2+3\gamma r+3)-(\gamma^2r^2+\gamma r+1)\right] e^{-\gamma r},$$

and

$$H_\rho = 0 \ ,$$

$$H_\phi = \frac{Id\ell\sin\theta}{4\pi r^2}\ (\gamma r+1)\ e^{-\gamma r} \ , \qquad \text{(II.15)}$$

$$H_z = 0 \ ,$$

where $\sin\theta = \rho/r$ and $\cos\theta = (z-\ell)/r$.

These latter expressions completely describe the electromagnetic fields produced in the medium by a current element source.

III. LINEAR CURRENT SOURCE OF FINITE LENGTH

Suppose now that we have an insulated thin straight wire extending from ℓ_1 to ℓ_2 on the z-axis of our coordinate system (Figure III.1) and carrying a current I $\exp(i\omega t)$, which we assume is constant throughout the length of the wire. The surrounding conducting medium is again assumed to be infinite and homogeneous with electric and magnetic properties σ, ε, and μ, as described in the previous section. We know that for a highly conducting medium such as sea water ($\sigma \simeq 4$ S/m) it is reasonable to neglect the displacement currents for all frequencies up to the microwave frequency range. We can therefore replace $(\sigma+i\omega\varepsilon)$ by σ in Equations (II.7) and (II.11), obtaining

$$\gamma \simeq (i\omega\mu\sigma)^{\frac{1}{2}} \tag{III.1}$$

$$\pi_z(\rho,z) \simeq \frac{Id\ell}{4\pi\sigma} \frac{e^{-\gamma r}}{r} \tag{III.2}$$

where, once again,

$$r = \left(\rho^2+(z-\ell)^2\right)^{\frac{1}{2}}.$$

III.1 Derivation of the Electric Field Components

In this subsection we follow the approach used by Wait [1952] to derive the components of the electric field produced by the finite linear current source. We start with the expression for the Hertz vector produced by a current element $Id\ell$ (Equation III.2). Integrating

from ℓ_1 to ℓ_2, we obtain the Hertz vector for a finite linear current source

$$\Pi_z(\rho,z) = \frac{1}{4\pi\sigma} \int_{\ell_1}^{\ell_2} \frac{I(\ell)e^{-\gamma r}}{r} \, d\ell \, . \tag{III.3}$$

Since we assumed that the current is constant throughout the wire, the Hertz vector can be rewritten as

$$\Pi_z(\rho,z) = \frac{I}{4\pi\sigma} \int_{\ell_1}^{\ell_2} \frac{e^{-\gamma r}}{r} \, d\ell \, . \tag{III.4}$$

Substituting this in Equation (II.12), it follows that the ρ and z components of the electric field are given by

$$E_\rho = - I \left[\frac{\partial Q(r)}{\partial \rho} \right]_{\ell = \ell_1}^{\ell_2} \, ,$$

$$E_z = - I \int_{\ell_1}^{\ell_2} P(r) d\ell - I \left[\frac{\partial Q(r)}{\partial z} \right]_{\ell = \ell_1}^{\ell_2} \, . \tag{III.5}$$

Here the function P(r) and Q(r) are defined [Sunde, 1949; Wait, 1952] as follows:

$$P(r) = \frac{i\omega\mu}{4\pi} \frac{e^{-\gamma r}}{r} \, ,$$

$$Q(r) = \frac{e^{-\gamma r}}{4\pi\sigma r} \, . \tag{III.6}$$

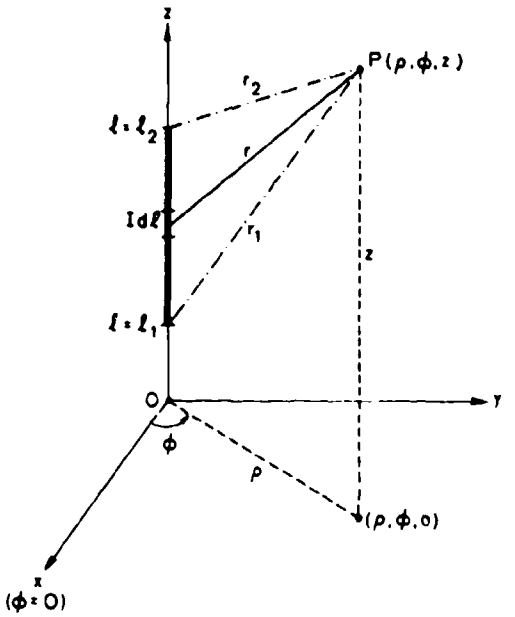

Figure III.1. Coordinate system and geometry used in the derivation of the electric and magnetic fields produced in a conducting medium of infinite extent by a linear current source of finite extent.

Making the following substitutions

$$\beta = 1/\delta = (\omega\mu\sigma/2)^{\frac{1}{2}}, \quad \gamma = (1+i)\beta ,$$

$$x = \beta(z-\ell), \quad a = \beta\rho ,$$

$$u = \left(a^2 + x^2\right)^{\frac{1}{2}} ,$$

the integral in Equation (III.5) can also be rewritten as

$$\int_{\ell_1}^{\ell_2} P(r)d\ell = -\frac{i\omega\mu}{4\pi}\int_{x_1}^{x_2} \frac{e^{-(1+i)u}}{u}\, dx , \qquad \text{(III.7)}$$

where $x_1 = \beta(z-\ell_1)$ and $x_2 = \beta(z-\ell_2)$.

This integral can be broken into three separate integrals:

$$\int_{x_1}^{x_2} \frac{e^{-(1+i)u}}{u}\, dx = \int_{x_1}^{x_2} \frac{1}{u}\, dx - \int_{x_1}^{x_2} \frac{1-e^{-u}\cos u}{u}\, dx - i\int_{x_1}^{x_2} \frac{e^{-u}\sin u}{u}\, dx .$$

Here the second and third integrals are the generalized cosine and sine integrals, $E_c[a,x]$ and $E_s[a,x]$, which are defined as follows:

$$E_c[a,x] = \int_0^x \frac{1-e^{-u}\cos u}{u}\, dx ,$$

$$E_s[a,x] = \int_0^x \frac{e^{-u}\sin u}{u}\, dx . \qquad \text{(III.8)}$$

Numerical values for these integrals are tabulated by Staff [1949].

The integral in Equation (III.5) can now be written

$$\int_{\ell_1}^{\ell_2} P(r)d\ell = -\frac{i\omega\mu}{4\pi}\left[\sinh^{-1}\frac{x}{a} - E_c[a,x] - iE_s[a,x]\right]_{x_1}^{x_2} . \qquad \text{(III.9)}$$

Combining Equations (III.5, III.6 and III.9), the following final expressions for the electric field components are obtained

$$E_\rho = \frac{\rho I}{4\pi\sigma}\left[\frac{e^{-\gamma r_2}}{r_2^3}(\gamma r_2+1) - \frac{e^{-\gamma r_1}}{r_1^3}(\gamma r_1+1)\right] \qquad \text{(III.10)}$$

and

$$E_z = \frac{i\omega\mu I}{4\pi}\left[\left\{\sinh^{-1}\frac{x_2}{a} - \sinh^{-1}\frac{x_1}{a} - E_c[a,x_2] + E_c[a,x_1]\right\} - i\left\{E_s[a,x_2] - E_s[a,x_1]\right\}\right] + \frac{I}{4\pi\sigma}\left[\frac{e^{-\gamma r_2}}{r_2^3}(\gamma r_2+1)(z-\ell_2) - \frac{e^{-\gamma r_1}}{r_1^3}(\gamma r_1+1)(z-\ell_1)\right], \qquad \text{(III.11)}$$

where $r_i (i=1,2)$ is given by $r_i = \left(\rho^2 + (z-\ell_i)^2\right)^{\frac{1}{2}}$.

III.2 Derivation of the Magnetic Field Component

To derive the magnetic field components produced by a linear current source of finite length, we substitute the expression for the Hertz vector derived in the previous section (Equation III.4) into

Equation (II.13). It follows that the magnetic field has only a single component H_ϕ given by

$$H_\phi = - \frac{\gamma^2}{i\omega\mu} \frac{I}{4\pi\sigma} \frac{\partial}{\partial\rho} \int_{\ell=\ell_1}^{\ell_2} \frac{e^{-\gamma r}}{r} \, d\ell \, , \qquad \text{(III.12)}$$

which can also be written as

$$H_\phi = - \frac{I}{4\pi} \int_{\ell=\ell_1}^{\ell_2} \left[\frac{\partial}{\partial\rho} \left(\frac{e^{-\gamma r}}{r} \right) \right] d\ell \, . \qquad \text{(III.13)}$$

Taking the derivative in the integral, we obtain

$$H_\phi = \frac{\rho I}{4\pi} \int_{\ell=\ell_1}^{\ell_2} \frac{e^{-\gamma r}(\gamma r+1)}{r^3} \, d\ell \, . \qquad \text{(III.14)}$$

Making the same substitutions as in the previous section, i.e., by writing

$$\beta = (\omega\mu\sigma/2)^{1/2}, \; \gamma = (1+i)\beta \, ,$$

$$x = \beta(z-\ell), \; a = \beta\rho \, ,$$

$$u = \left(a^2 + x^2 \right)^{1/2} \, ,$$

Equation (III.14) can be written as

$$H_\phi = - \frac{\rho\beta^2 I}{4\pi} \int_{x_1}^{x_2} \left[\frac{(1+i)e^{-(1+i)u}}{u^2} + \frac{e^{-(1+i)u}}{u^3} \right] dx \qquad \text{(III.15)}$$

where, once again, $x_1 = \beta(z-\ell_1)$ and $x_2 = \beta(z-\ell_2)$. This integral can be decomposed into the following form:

$$H_\varphi = -\frac{\rho\beta^2 I}{4\pi}\left[\left\{\int_{x_1}^{x_2}\frac{e^{-u}\cos u}{u^2}\,dx + \int_{x_1}^{x_2}\frac{e^{-u}\sin u}{u^2}\,dx + \int_{x_1}^{x_2}\frac{e^{-u}\cos u}{u^3}\,dx\right\} + i\left\{\int_{x_1}^{x_2}\frac{e^{-u}\cos u}{u^2}\,dx - \int_{x_1}^{x_2}\frac{e^{-u}\sin u}{u^2}\,dx - \int_{x_1}^{x_2}\frac{e^{-u}\sin u}{u^3}\,dx\right\}\right].$$

At this stage, we will define four different integrals as follows:

$$M_c[a,x] = \int_0^x \frac{e^{-u}\cos u}{u^2}\,dx\,,$$

$$M_s[a,x] = \int_0^x \frac{e^{-u}\sin u}{u^2}\,dx\,, \qquad \text{(III.16)}$$

$$N_c[a,x] = \int_0^x \frac{e^{-u}\cos u}{u^3}\, dx \ ,$$

$$N_s[a,x] = \int_0^x \frac{e^{-u}\sin u}{u^3}\, dx \ .$$

Using these integrals, the magnetic field expression can be written as

$$H_\phi = -\frac{\rho\beta^2 I}{4\pi}\left[\left\{M_c[a, x_2] - M_c[a, x_1] + M_s[a, x_2] - M_s[a, x_1] + N_c[a, x_2] - N_c[a, x_1]\right\} + i\left\{M_c[a, x_2] - M_c[a, x_1] - M_s[a, x_2] + M_s[a, x_1] - N_s[a, x_2] + N_s[a, x_1]\right\}\right] \qquad \text{(III.17)}$$

with the corresponding component of magnetic induction B_ϕ being given by the usual expression

$$B_\phi = \mu_0 H_\phi \ . \qquad \text{(III.18)}$$

III.3 Parametric Approach

As shown by Fraser-Smith and Bubenik [1979], we can make use of a parametric approach by normalizing all the distances in our expressions by the skin depth of the surrounding conducting medium, δ, where

$$\delta = \frac{1}{\beta} = (2/\omega\mu\sigma)^{\frac{1}{2}} \ .$$

Using this technique, Equations (III.10), (III.11) and (III.17) can be written in the following forms:

$$\sigma\delta^2 E_\rho = \frac{\rho_\delta I}{4\pi} \left[\frac{e^{-(1+i)r_{2\delta}}}{r_{2\delta}^3} \left((1+i)r_{2\delta}+1\right) - \frac{e^{-(1+i)r_{1\delta}}}{r_{1\delta}^3} \left((1+i)r_{1\delta}+1\right)\right], \quad \text{(III.19)}$$

$$\sigma\delta^2 E_z = \frac{iI}{2\pi} \left[\left\{ \sinh^{-1} \frac{z_\delta - \ell_{2\delta}}{\rho_\delta} - \sinh^{-1} \frac{z_\delta - \ell_{1\delta}}{\rho_\delta} \right.\right.$$

$$\left. - E_c \left[\rho_\delta, (z_\delta - \ell_{2\delta})\right] + E_c \left[\rho_\delta, (z_\delta - \ell_{1\delta})\right] \right\}$$

$$\left. - i \left\{ E_s \left[\rho_\delta, (z_\delta - \ell_{2\delta})\right] - E_s \left[\rho_\delta, (z_\delta - \ell_{1\delta})\right] \right\} \right]$$

$$+ \frac{I}{4\pi} \left[\frac{e^{-(1+i)r_{2\delta}}}{r_{2\delta}^3} \left((1+i)r_{2\delta}+1\right) \left(z_\delta - \ell_{2\delta}\right) - \frac{e^{-(1+i)r_{1\delta}}}{r_{1\delta}^3} \right.$$

$$\left. \left((1+i)r_{1\delta}+1\right) \left(z_\delta - \ell_{1\delta}\right) \right] , \quad \text{(III.20)}$$

$$\delta H_\phi = -\frac{\rho_\delta I}{4\pi}\left[\left\{M_c\left[\rho_\delta, (z_\delta - \ell_{2\delta})\right] - M_c\left[\rho_\delta, (z_\delta - \ell_{1\delta})\right]\right.\right.$$
$$+ M_s\left[\rho_\delta, (z_\delta - \ell_{2\delta})\right] - M_s\left[\rho_\delta, (z_\delta - \ell_{1\delta})\right]$$
$$\left.\left. + N_c\left[\rho_\delta, (z_\delta - \ell_{2\delta})\right] - N_c\left[\rho_\delta, (z_\delta - \ell_{1\delta})\right]\right\}\right.$$
$$+ i\left\{M_c\left[\rho_\delta, (z_\delta - \ell_{2\delta})\right] - M_c\left[\rho_\delta, (z_\delta - \ell_{1\delta})\right]\right.$$
$$- M_s\left[\rho_\delta, (z_\delta - \ell_{2\delta})\right] + M_s\left[\rho_\delta, (z_\delta - \ell_{1\delta})\right]$$
$$\left.\left. - N_s\left[\rho_\delta, (z_\delta - \ell_{2\delta})\right] + N_s\left[\rho_\delta, (z_\delta - \ell_{1\delta})\right]\right\}\right], \qquad \text{(III.21)}$$

where

$$\rho_\delta = \rho/\delta, \quad z_\delta = z/\delta,$$
$$\ell_{1\delta} = \ell_1/\delta, \quad \ell_{2\delta} = \ell_2/\delta, \qquad \text{(III.22)}$$
$$r_{1\delta} = r_1/\delta, \quad r_{2\delta} = r_2/\delta.$$

Note that the ρ_δ introduced here is the same as the quantity a used previously; we introduce ρ_δ solely for notational consistency.

These parametric equations (i.e., Equations III.19, III.20, and III.21) may be used to convert the field values calculated for one particular frequency to another set of field values at some other frequency without much additional computation. For example, assume that the values of the electric and magnetic fields produced by the linear current source

at the observation point $P(\rho, \phi, z)$ in Figure III.1 are known for a certain frequency f_1. Let these field values be $E_\rho = E_{\rho 1}$, $E_z = E_{z1}$ and $B_\phi = B_{\phi 1}$ respectively. If we now change the frequency by a factor $1/A^2$ to $f_2 = f_1/A^2$ the new skin depth will be $\delta_2 = A\delta_1$. If we multiply all the distance coordinates in Figure III.1 by A, i.e., change ℓ_1, ℓ_2, ρ, and z to $A\ell_1$, $A\ell_2$, $A\rho$, and Az, then all the normalized distances in the parametric equations stay the same and the electric and magnetic field components at the new observation point P $(A\rho, \phi, Az)$ produced by the linear current source extending from $\ell = A\ell_1$ to $\ell = A\ell_2$ and operating at the new frequency $f_2 = f_1/A^2$ become $E_{\rho 2} = E_{\rho 1}/A^2$, $E_{z2} = E_{z1}/A^2$ and $B_{\phi 2} = B_{\phi 1}/A$. These new field values for frequency f_2 can obviously be calculated more easily from the field values for frequency f_1 than they can from the original integral expressions.

III.4 Computations of the Fields

The expressions derived in Sections III.1 and III.2 for the field components E_z and B_ϕ contain integrals which in general can only be evaluated numerically. As mentioned in Section III.1, there are a limited number of tabulated values available [Staff, 1949] for the two integrals $E_c[a,x]$ and $E_s[a,x]$ in the expression for E_z, but there are no tabulated values for the four integrals $M_c[a,x]$, $M_s[a,x]$, $N_c[a,x]$, and $N_s[a,x]$ in the expression for B_ϕ. We therefore prepared two computer programs for evaluating (1) the two components of the electric field, E_ρ and E_z, and (2) the component of the magnetic field, B_ϕ. In these programs the six constitutive integrals in the field expressions were

evaluated numerically by means of Weddle's rule [Scarborough, 1966, p. 138]. Both programs were interactive in the sense that the value of a field component could be evaluated by entering the location and the length of the linear current source, the amplitude and the frequency of the current flowing in the source, and the coordinates of the observation point in the surrounding conducting medium.

The values for the numerical integrals were checked in several different ways. One obvious way was by comparing our computed results for $E_c[a,x]$ and $E_s[a,x]$ with the available tabulated values [Staff, 1949]. Another way was to see if the values of the integrals converged to the values tabulated for Kelvin functions and their derivatives [Young and Kirk, 1964; Lowell, 1959; see Appendix B] for large values of the upper limit of these integrals. We also used Simpson's rule [Scarborough, 1966, p. 137] and compared the values obtained by two different methods of numerical integration; namely, Weddle's rule and Simpson's rule. In all cases our computed values agreed well with the comparison values.

Shown in Figures III.2 to III.7 are computed values of the electric and magnetic fields produced at frequencies of 100 Hz (Figures III.2, III.4 - III.7) and 1 Hz (Figures III.3, III.8) by a linear current source of 100 m length carrying an alternating current of 1000 A amplitude. The fields are shown in two dimensions; in all cases the fields are cylindrically symmetric about the axis defined by the source. Figures III.2 and III.3 show the spatial variations of the total electric field vector at the instant when there is maximum current (1000A) in the source flowing from B to A. The shorter wavelength at 100 Hz can

be clearly seen when comparison is made of the two figures. Figure III.4 shows equal amplitude contours of the magnetic field component B_ϕ for a frequency of 100 Hz at the time instant of maximum current flow from B to A. Figures III.5 and III.6 show contours of the maximum values reached by the two components of the electric field E_z and E_ρ during one cycle of the source current. The dashed contours indicated zero amplitude; thus in Figure III.6 the E_ρ component is zero along the axis of the source and along the perpendicular line through the center of the source. Comparing the two electric field figures, it is easy to see how the two separate components E_z and E_ρ contribute to the total electric field.

In Figure III.7 we have drawn contours indicating the maximum values reached by the 100 Hz total magnetic field variation at each point during one cycle. Thus at points inside the contour labelled 10^4 pT, our data show that the total magnetic field (or, equivalently, the magnetic field component B_ϕ) will reach a values of 10^4 pT or more during one cycle of the source current.

In Figure III.8 we have relabelled the data in Figure III.7 according to the parametric approach described in Section III.3; the frequency has been decreased by a factor of 100, the distances have been increased by a factor of 10, and the values of B_ϕ on the contours have been decreased by a factor of 10. These changes leave the basic figure unaltered, but the various contours now show maximum total magnetic field values produced by a source of 1000 m length carrying a 1000 A alternating current with a frequency of 1 Hz.

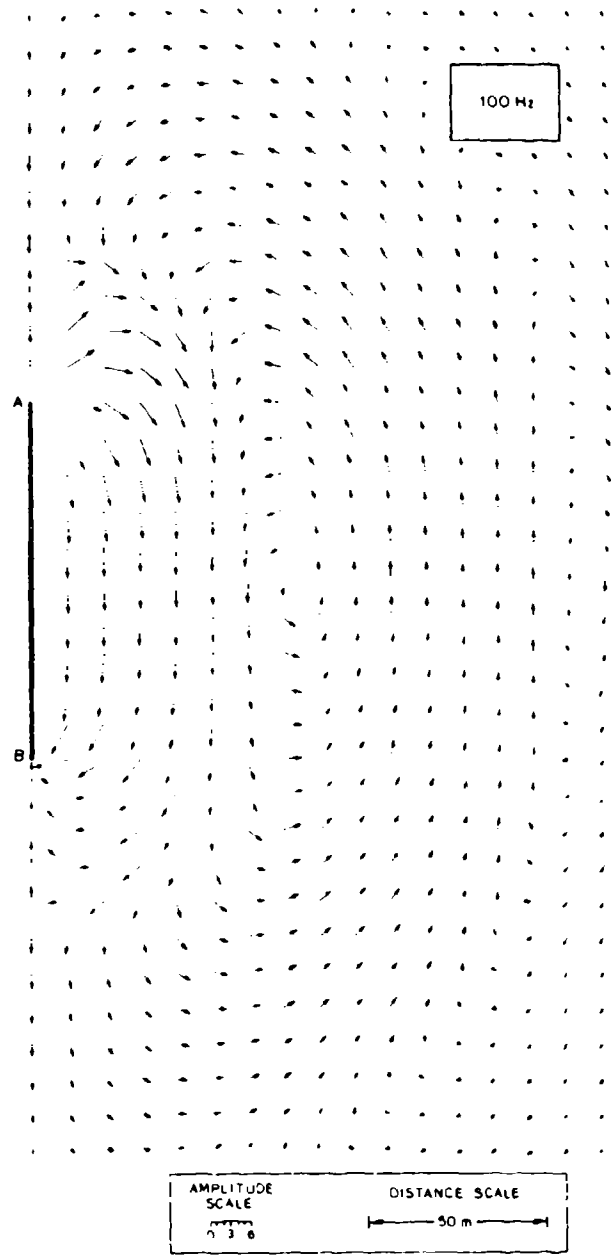

Figure III.2. Variation of the total electric field vector produced in sea water by a linear current source of finite length (100 m) carrying an alternating current of amplitude 1000 A and frequency 100 Hz at the time instant when there is maximum current flowing in the direction from B to A. The magnitude of the electric field vector is 10^n μv/m, where n can be read from the amplitude scale shown above. The pattern of electric field vectors is cylindrically symmetric around the axis of the source.

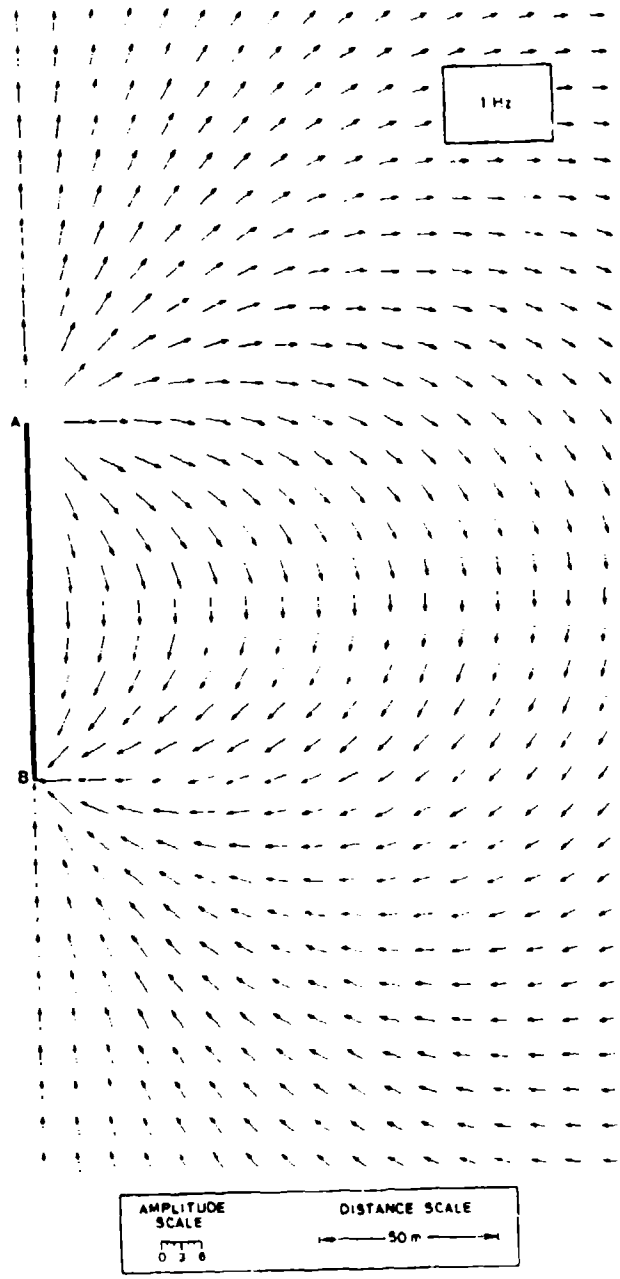

Figure III.3. Variation of the total electric field vector produced in sea water by a linear current source of finite length (100 m) carrying an alternating current of amplitude 1000 A and frequency 1 Hz at the time instant when there is maximum current flowing in the direction from B to A. The magnitude of the electric field vector is 10^n μv/m, where n can be read from the amplitude scale shown above. The pattern of electric field vectors is cylindrically symmetric around the axis of the source.

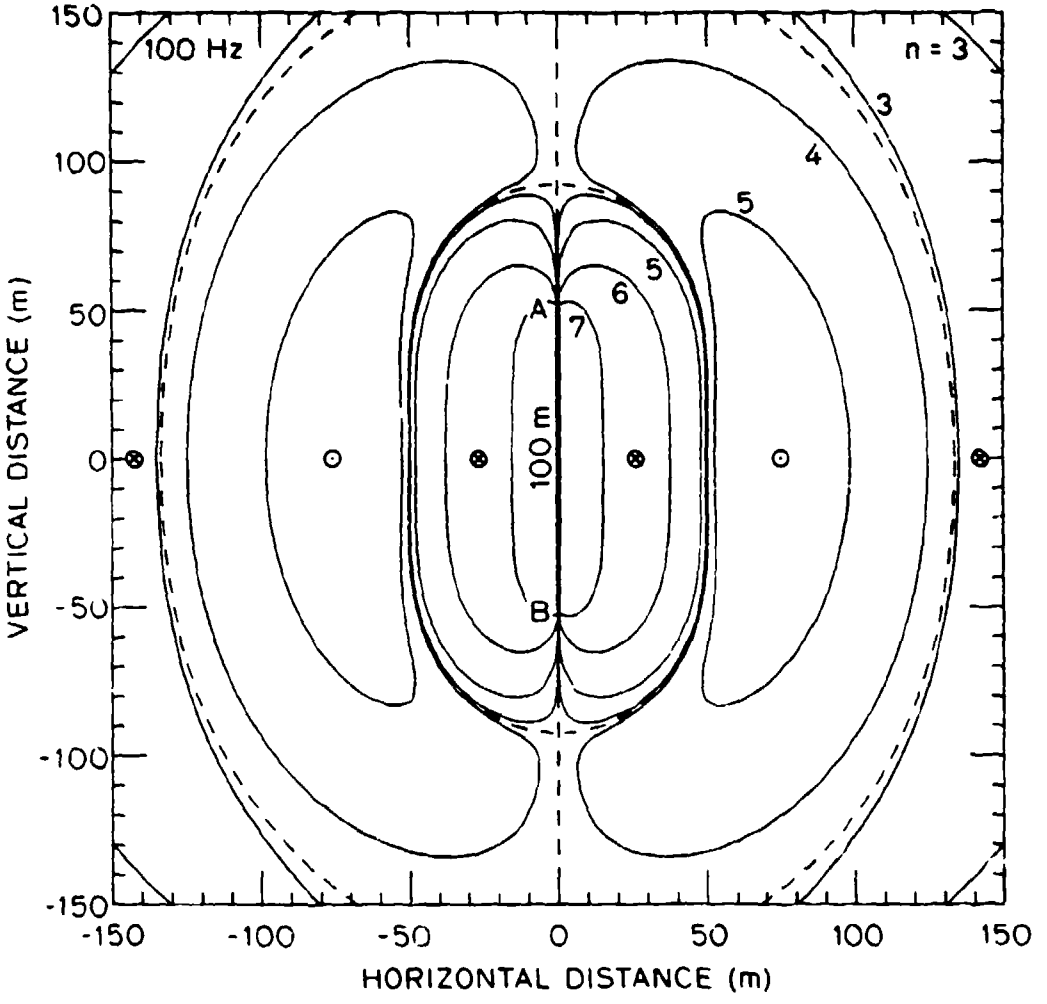

Figure III.4. Variation of the total magnetic field (which has only the one component B_ϕ) produced in sea water by a linear current source of finite length (100 m) carrying an alternating current of amplitude 1000 A and frequency 100 Hz at the time instant when there is maximum current flowing in the direction from B to A. The magnetic field magnitudes are given by $B_\phi = 10^n$ pT, where n is given for each contour in the figure (B_ϕ = 0 on the dashed contours.) As indicated, the direction of B_ϕ is either into the paper or out of the paper depending on the region between the dashed lines. The field pattern is cylindrically symmetric around the axis of the source.

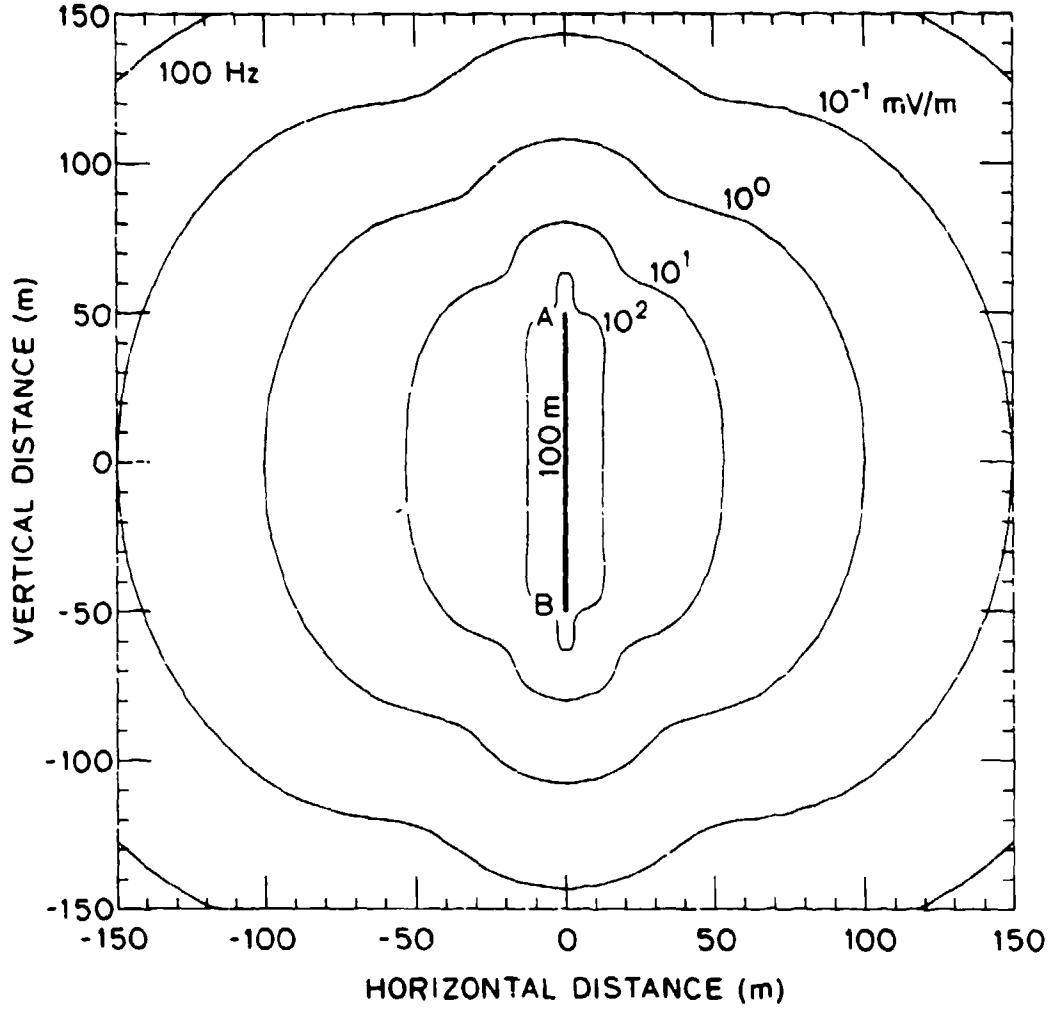

Figure III.5. Variation of the amplitude of the parallel component of the electric field, E_z, produced in sea water by a linear current source of finite length (100 m) carrying an alternating- current of amplitude 1000 A and frequency 100 Hz. The amplitude of E_z is constant along each contour. The field pattern is cylindrically symmetric around the axis of the source.

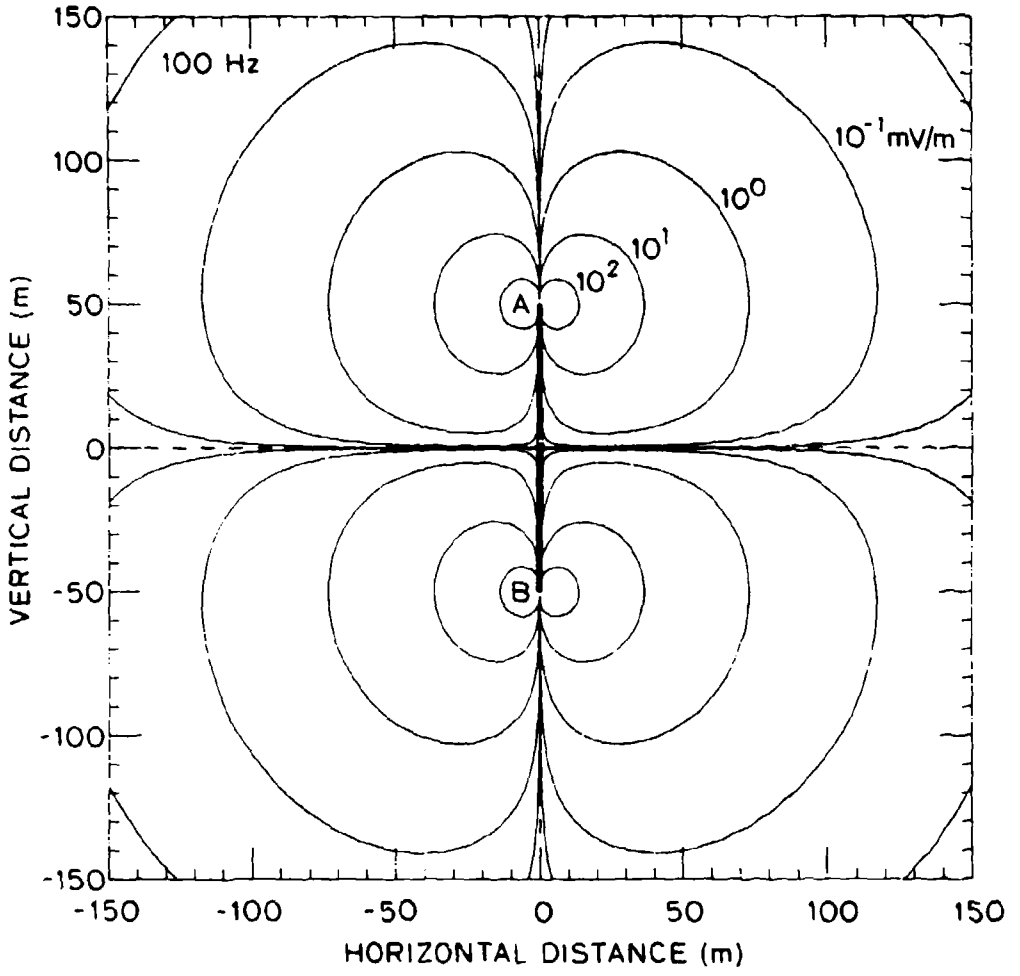

Figure III.6. Variation of the amplitude of the perpendicular component of the electric field, E_ρ, produced in sea water by a linear current source of finite length (100 m) carrying an alternating current of amplitude 1000 A and frequency 100 Hz. The amplitude of E_ρ is constant along each contour and is zero along the dashed lines. The field pattern is cylindrically symmetric around the axis of the source.

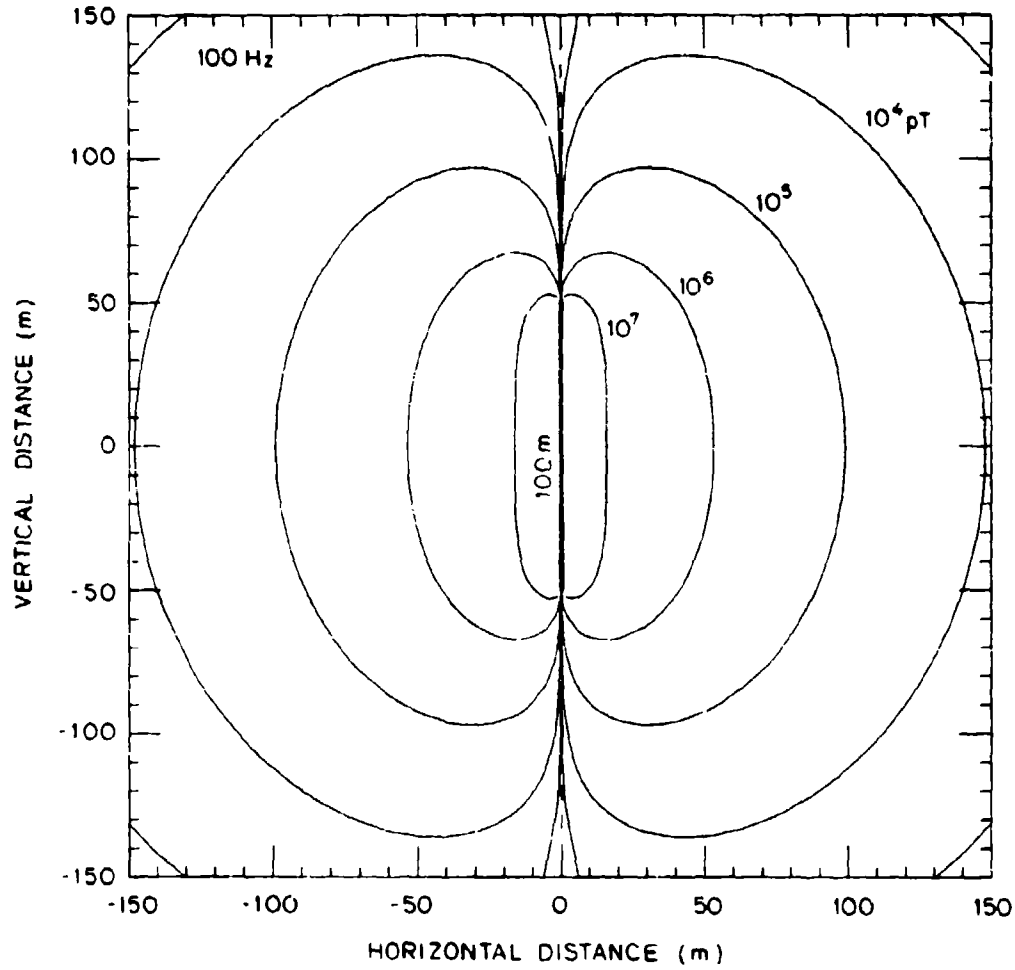

Figure III.7. Variation of the amplitude of the total magnetic field (which has only the one component B_ϕ) produced in sea water by a linear current source of finite length (100 m) carrying an alternating current of amplitude 1000 A and frequency 100 Hz. The field pattern is cylindrically symmetric around the axis of the source.

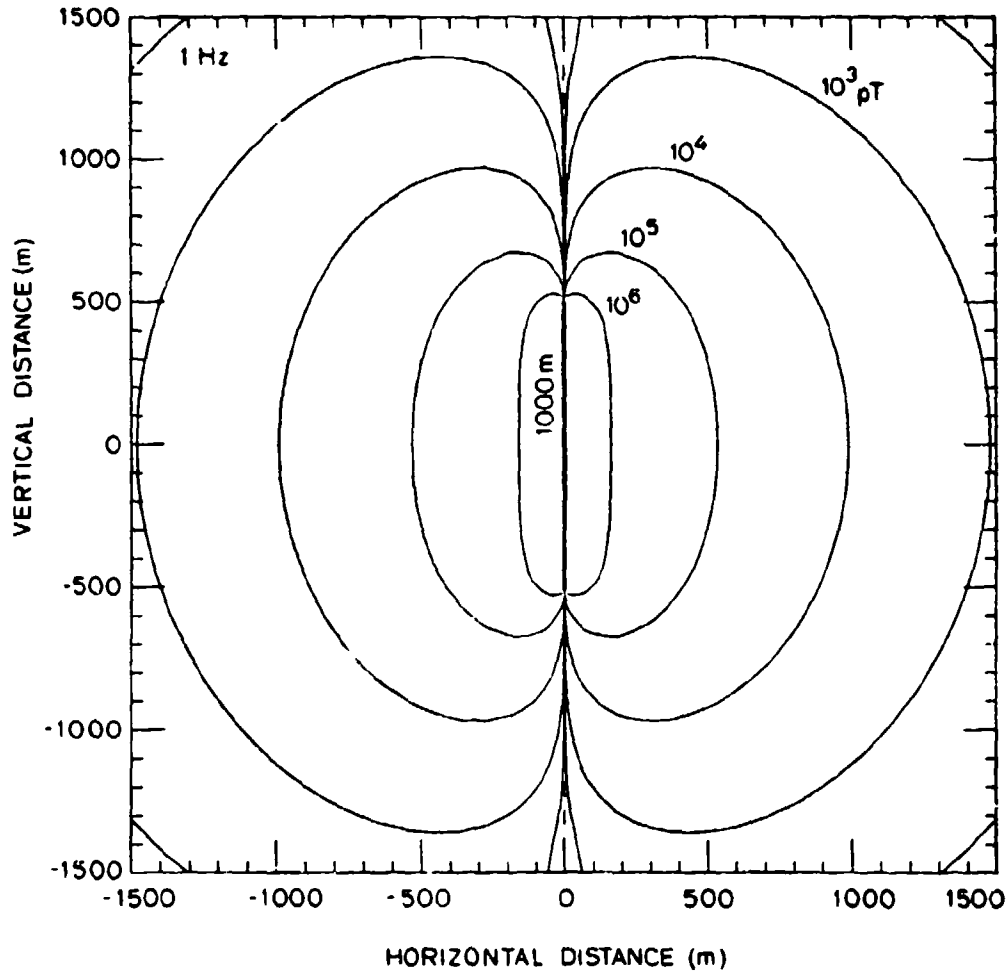

Figure III.8. Variation of the amplitude of the total magnetic field produced in sea water by a linear current source of finite length (1000 m) carrying an alternating current of amplitude 1000 A and frequency 1 Hz. The field pattern is cylindrically symmetric around the axis of the source and is identical to the pattern shown in Figure III.7 for a frequency of 100 Hz; however, the scales have been changed in accordance with the rules for the parametric approach described in the text.

Finally, in Figures III.9 and III.10 we have plotted data that compare the electric and magnetic fields produced by the finite source with those produced by an infinite source carrying the same current. Comparison of the electric fields is made in Figure III.9, where we show the variation with distance (along the perpendicular axis through the center of the finite source) of the ratio of the amplitudes of the z-components of the electric field produced by the finite (length 100 m) and infinite sources. Because of the choice of the central axis to show the distance variation, the E_z component for the finite source is also the total electric field; we already know, of course, that the E_z component for the infinite source is everywhere the same as the total field. Thus the ratio of the E_z components shown in the figure is also the ratio of the total electric fields. Figure III.10 shows the variation of the ratio of the amplitudes of the total magnetic field (i.e., its single component B_ϕ) for the same two sources.

An interesting feature of the electric field data in Figure III.9 is the relative enhancement of the electric fields near the source of finite length. The increase only becomes apparent for frequencies less than 10 Hz, but it increases rapidly with decreasing frequency and can be of the order 10^3 at f = 0.001 Hz. The ratio of the magnetic fields, on the other hand, never exceeds unity near the source and it decreases with increasing distance from the source.

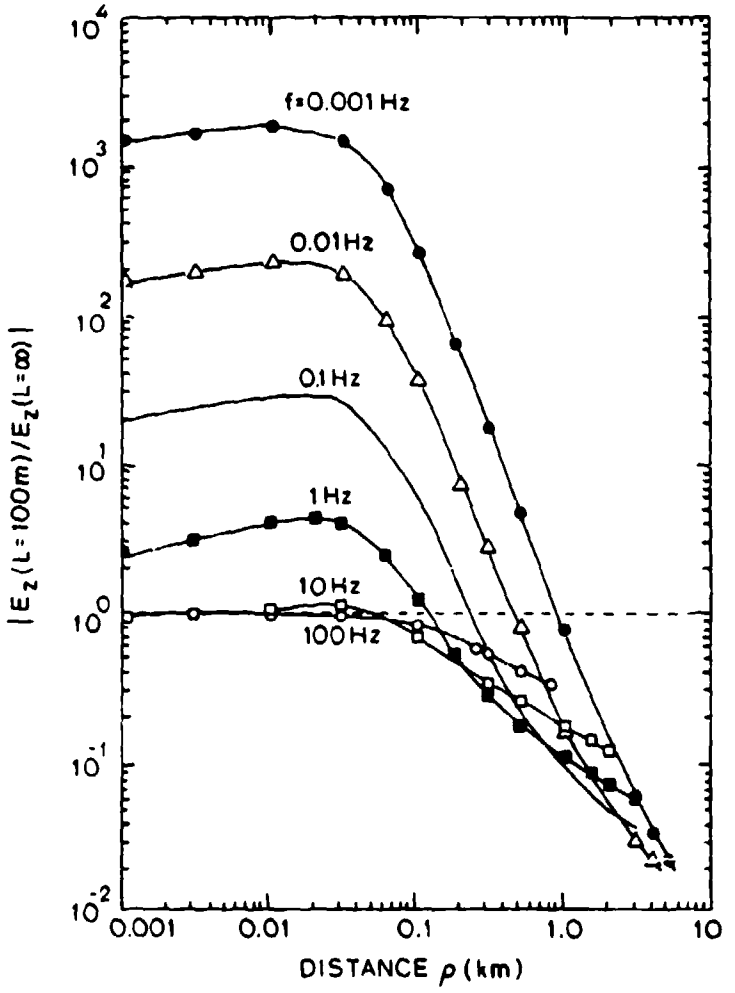

Figure III.9. Variation with perpendicular distance of the ratio of the amplitude of the z-component of the electric field produced by a linear current source of finite length (100 m) to the amplitude of the z-component of the electric field produced by a linear current source of infinite length, both carrying alternating currents of the same amplitude and frequency. The particular perpendicular axis along which the variation is shown passes through the center of the finite source. The surrounding conducting medium (sea water, σ = 4 S/m) is infinite in extent. Each curve refers to a different frequency in the range 0.001-100 Hz as shown in the figure.

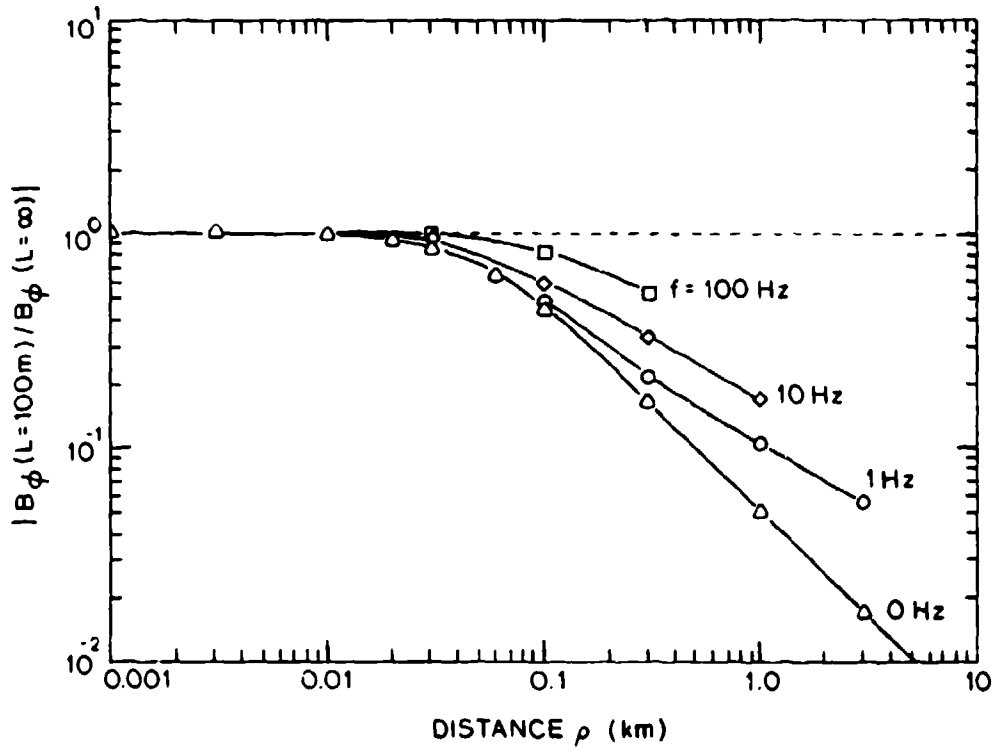

Figure III.10. Variation with perpendicular distance of the ratio of the amplitude of the magnetic field produced by a linear current source of finite length (100 m) to the amplitude of the magnetic field produced by a linear current source of infinite length, both carrying alternating currents of the same amplitude and frequency. The particular perpendicular axis along which the variation is shown passes through the center of the finite source. The surrounding conducting medium (sea water, σ = 4 S/m) is infinite in extent. Each curve refers to a different frequency in the range 0 - 100 Hz as shown in the figure.

IV. LINEAR CURRENT SOURCE OF INFINITE LENGTH

IV.1 Derivation of the Field Expressions

In the preceding section we derived expressions for the electric and magnetic fields produced in a conducting medium of infinite extent by a linear current source of finite length. In the coordinate system of Figure III.1 the wire extended from ℓ_1 to ℓ_2 in the z direction. Suppose now that we let ℓ_1 go to $-\infty$ and ℓ_2 go to $+\infty$. The electric field components given by Equations III.5 then become

$$E_\rho = 0 \ ,$$

$$E_z = -I \int_{-\infty}^{\infty} P(r) d\ell \ . \tag{IV.1}$$

Thus the electric field of a linear current source of infinite length aligned in the z direction has only a z-component. Making the same substitution as in Section III, the expression for E_z can also be written as

$$E_z = \frac{i\omega\mu I}{4\pi} \int_{\infty}^{-\infty} \frac{e^{-(1+i)u}}{u} dx \ ,$$

where $u = (a^2 + x^2)^{\frac{1}{2}}$. Knowing that the integral in this equation is an even function of x, we can also write

$$E_z = \frac{-i\omega\mu I}{2\pi} \int_0^{\infty} \frac{e^{-(1+i)u}}{u} dx \ . \tag{IV.2}$$

As described in Appendix B, the integral can be replaced by the modified

Bessel function of the second kind of order zero, $K_0(\gamma\rho)$, giving

$$E_z = \frac{-\gamma^2 I}{2\pi\sigma} K_0(\gamma\rho), \qquad \text{(IV.3)}$$

which is the same expression as that derived by Von Aulock [1948] and by Wait [1959].

To derive the magnetic field, we make use of the above results for the electric field and Maxwell's Equation (II.3). After appropriate algebraic manipulation we obtain the following expression for the single magnetic field intensity component H_ϕ:

$$H_\phi = - \frac{i}{\omega\mu} \frac{\partial E_z}{\partial \rho} .$$

Differentiation of Equation (IV.3) then gives

$$H_\phi = \frac{\gamma I}{2\pi} K_1(\gamma\rho), \qquad \text{(IV.4)}$$

where $K_1(\gamma\rho)$ is the modified Bessel function of the second kind of order one. This latter expression for the magnetic field intensity was also derived by Von Aulock [1948] and by Wait [1959].

Summarizing the above results, we see that a wire of infinite length carrying a uniform current $I \exp(i\omega t)$ along the z axis in an infinite, homogeneous, conducting medium produces an electric field with a single component in the z direction (i.e., directed parallel to the wire) given by Equation (IV.3) and a magnetic field with a single component in the ϕ direction (i.e., azimuthal component) given by Equation (IV.4).

IV.2 Effects of Insulation

In the preceding derivations of the field expressions for linear

current sources of finite and infinite length we assume that the current is uniform throughout the length of the conducting wire comprising the actual source and that it flows into the conducting medium only from the ends of the wire. For this condition of uniform current to apply, it is of course necessary to have insulation on the wire. Without insulation the current in the wire would flow into the surrounding conducting medium from all points of the wire's surface, and uniform current flow along the length of the wire could not be achieved.

Extending results obtained by Sunde [1949], Wait [1952] states that the propagation constant for low frequency currents in an insulated wire in a conducting medium is determined largely by the electrical characteristics of the insulation, and he gives the following approximate expression for the current $I(x)$ at a point in the wire located a distance x away from the generator terminals:

$$I(x) \approx I_0 \exp(-\Gamma x),$$

where I_0 is the current assumed to be entering the wire. The propagation constant Γ in this expression is given approximately by

$$\Gamma \approx i(\varepsilon_i \mu_i \omega^2)^{\frac{1}{2}},$$

where ε_i and μ_i are the permittivity and permeability of the insulation material. It follows from these expressions that the current along an insulated wire of length L will be essentially uniform provided $|\Gamma L| \ll 1$. Suppose we take polyethylene to be a typical insulating material. For this material we can write $\varepsilon_i = \varepsilon_r \varepsilon_0$, with $\varepsilon_r = 2.25$ (the dielectric constant of polyethylene), and $\mu = \mu_0$. Substituting the known values of

ε_0 and μ_0, we obtain

$$|\Gamma| \approx (3.14 \times 10^{-8} f)\ m^{-1}\ ,$$

For $f = 1$ Hz, $|\Gamma| \approx 3 \times 10^{-8}\ m^{-1}$ and the length of wire can be as large as 1000 km and yet the condition $|\Gamma L| << 1$ is still satisfied. Thus for low frequencies and typical insulating materials, it is reasonable to assume that an alternating current is uniform throughout the length of a wire for wire lengths varying from several hundreds to several thousands of kilometers.

It also follows that the displacement currents flowing to the surrounding medium through the insulation are negligible and the current mostly flows to the medium from the ends of the wire.

It is also shown analytically by Wait [1952] and stated by Kraichman [1976] that the electric and magnetic field expressions for linear current sources of both finite and infinite length (with the wire assumed to be of negligible thickness in both cases) are unaffected by the properties of the insulating material on the wire as long as the ratio of the radius of the insulation to the wavelength of the surrounding conducting medium is much less than one. This condition can be written in the form

$$b(f\mu\sigma)^{\frac{1}{2}} << 1,$$

where b is the radius of insulation and μ and σ are the permeability and the conductivity of the surrounding medium. For sea water ($\sigma = 4$ S/m, $\mu = \mu_0 = 4\pi \times 10^{-7}$ H/m) this condition becomes

$$2.24 \times 10^{-3}\ b\ f^{\frac{1}{2}} << 1,$$

which will of course be satisfied for low frequencies and reasonable thickness of insulation.

IV.3 Computation of the Fields

Plots of the variations with distance of the amplitudes of E_z and H_ϕ produced in sea water by linear current sources of infinite length are given by Von Aulock [1948] and Kraichman [1976] for a few selected frequencies and for limited ranges of magnitude and distance. These data play such an important role in the study of the electric and magnetic fields produced in sea water by submerged linear current sources that we have extended the Von Aulock/Kraichman curves over a number of decades in frequency, amplitude and distance.

In our derivation of the numerical data for these curves, we made use of the fact that Equations (IV.3) and (IV.4) can be rewritten in terms of the Kelvin functions and their derivations to give the following two new equations

$$E_z = - \frac{i\omega\mu I}{2\pi} \left[\ker_0 \left(\sqrt{2}\, a\right) + i\, \mathrm{kei}_0 \left(\sqrt{2}\, a\right) \right] , \qquad \text{(IV.5)}$$

and

$$H_\phi = - \frac{\beta I}{\sqrt{2}\,\pi} \left[\ker_0' \left(\sqrt{2}\, a\right) + i\, \mathrm{kei}_0' \left(\sqrt{2}\, a\right) \right] , \qquad \text{(IV.6)}$$

where $a = \beta\rho$ and $\rho = (\omega\mu c/2)^{\frac{1}{2}}$, as before. It follows that E_z and H_ϕ can be evaluated either by using tables of the Kelvin functions and their derivatives [Lowell, 1959; Young and Kirk, 1964] in conjunction with Equations (IV.5) and (IV.6), or by using numerical integration techniques. We used both methods to obtain our numerical values for the amplitudes of E_z and H_ϕ.

The curves we obtained for the variation of the amplitude of the electrical field component E_z with frequency and perpendicular distance from the wire are shown in Figure IV.1, and the corresponding curves for the amplitude of the magnetic field component B_ϕ are shown in Figure IV.2. In these curves the lower limits of the amplitudes, 10^{-3} mV/m for the electrical field and 10^{-1} pT for the magnetic field, are roughly the smallest values that can be measured at depth in the sea with present technology.

There is an interesting feature of the electric field variation that particularly distinguishes it from the magnetic field variation: the electric field first increases, reaches a maximum value, and then decreases with increasing frequency, whereas the magnetic field decreases monotonically with increasing frequency. This feature can be seen more clearly when the variation of the amplitude of the electric field is plotted against frequency, as shown in Figure IV.3, and it implies that, for a given perpendicular distance between the source and the field point, there is an optimum frequency at which the amplitude of the electric field is a maximum at the field point.

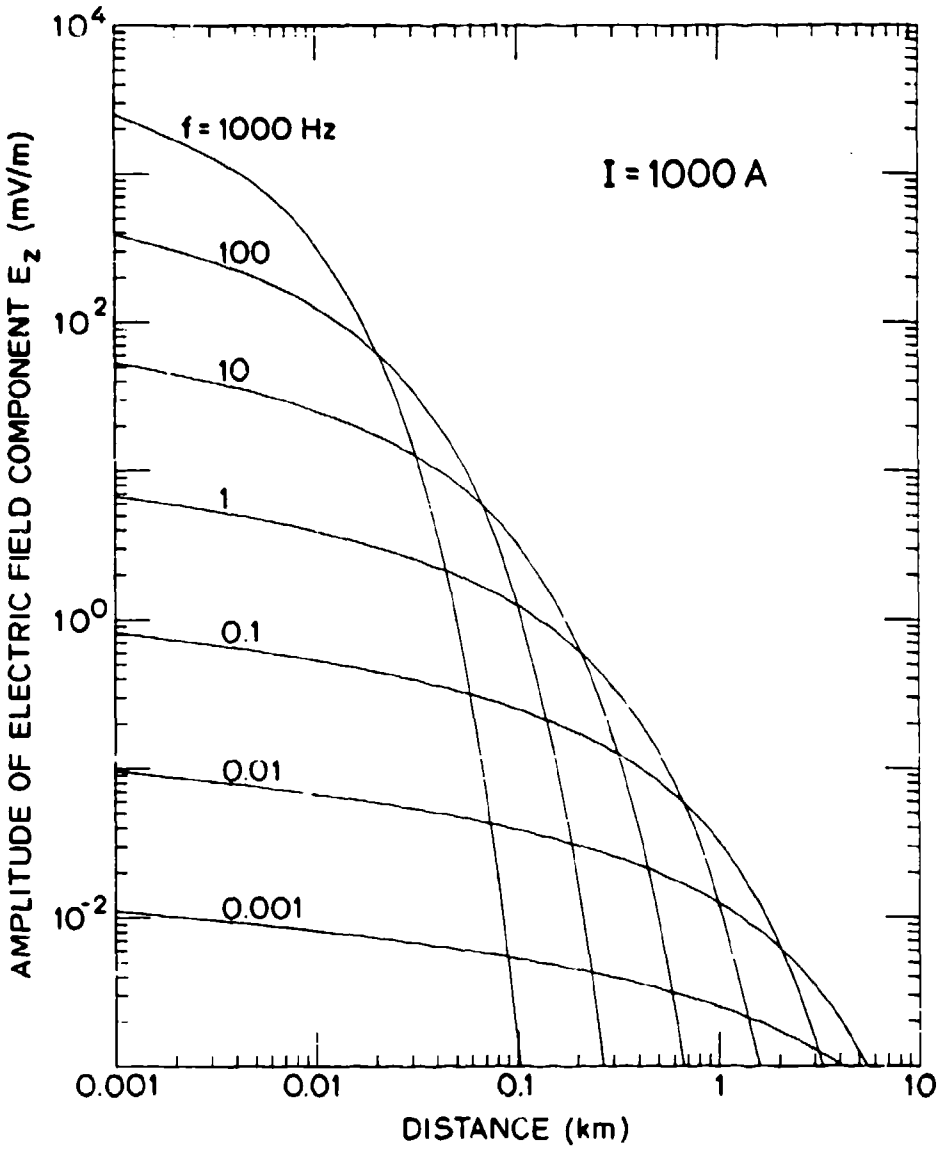

Figure IV.1. Variation with perpendicular distance of the amplitude of the electric field produced in sea water by a linear current source of infinite length carrying an alternating current of amplitude 1000A. The electric field amplitudes for an arbitrary current I can be derived from the values given above by multiplying by I/1000.

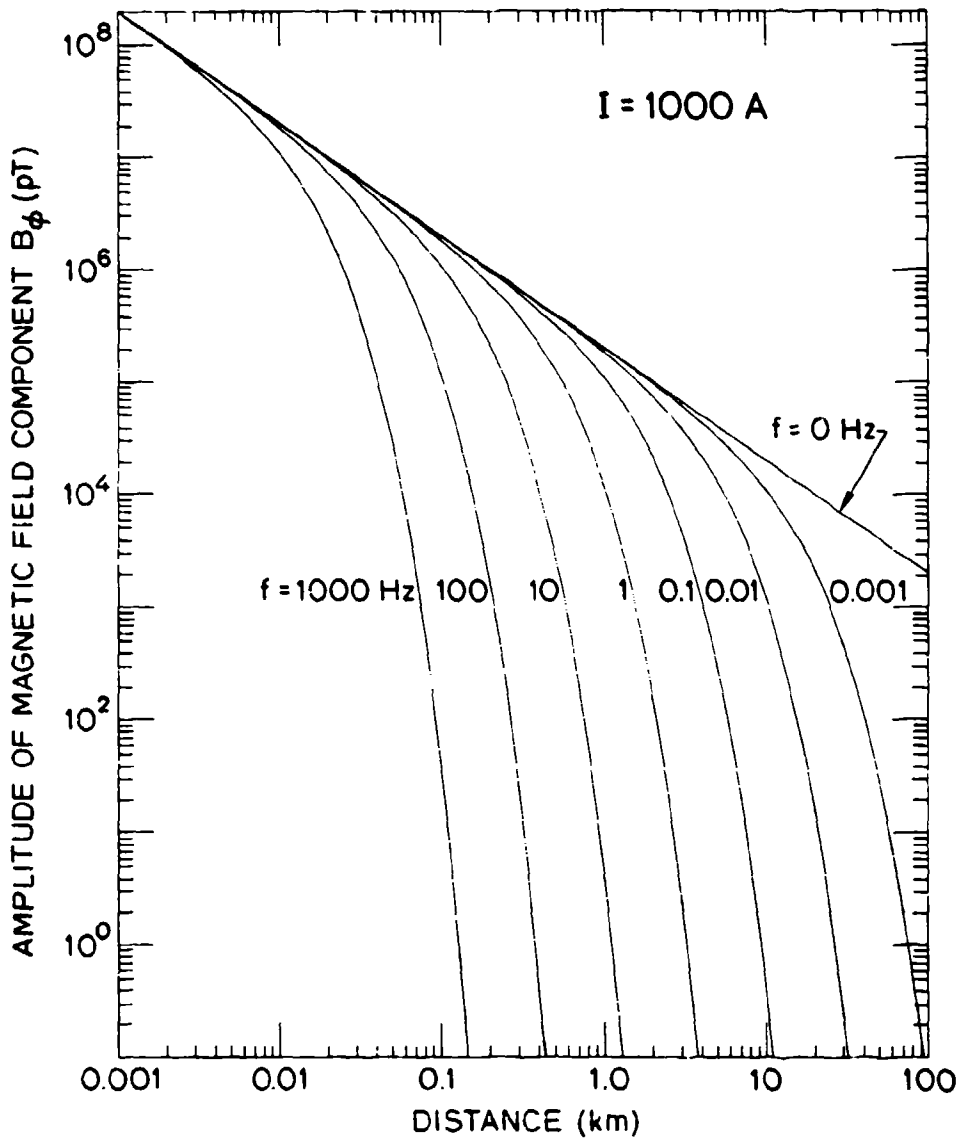

Figure IV.2. Variation with perpendicular distance of the amplitude of the magnetic field produced in sea water by a linear current source of infinite length carrying an alternating current of amplitude 1000 A. The magnetic field amplitudes for an arbitrary current I can be derived from the values given above by multiplying by I/1000.

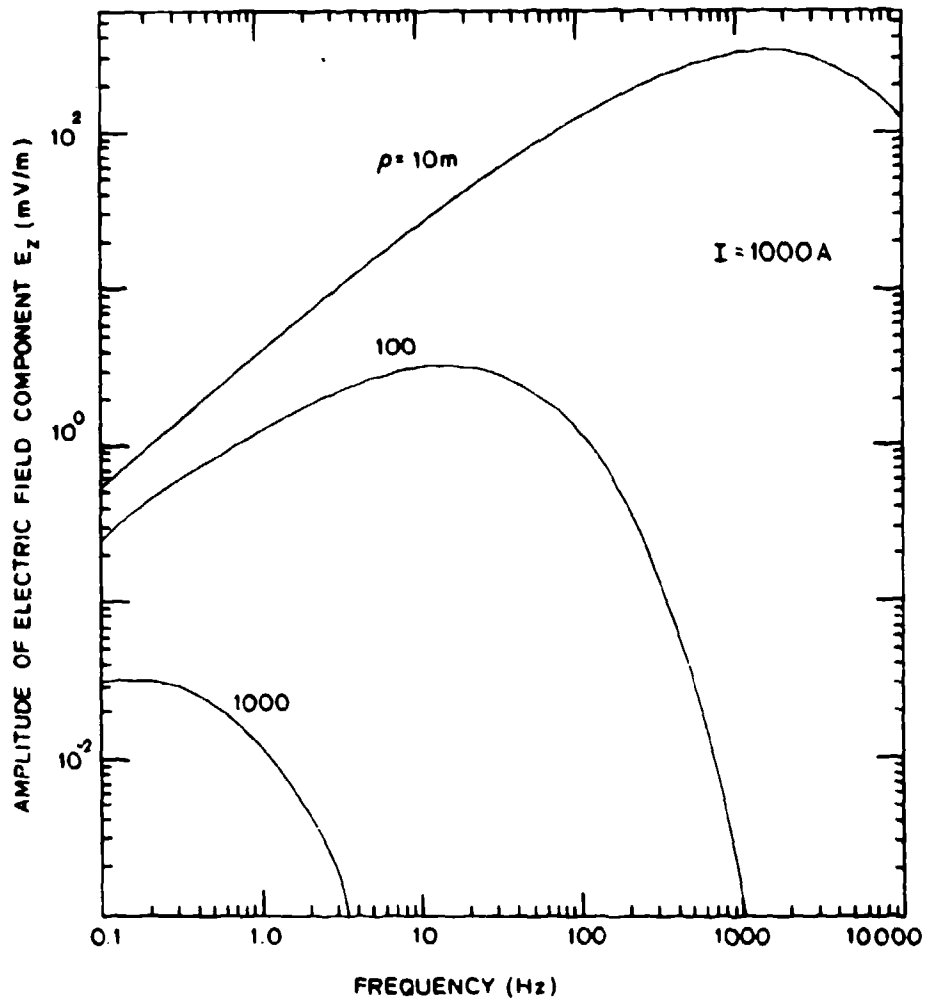

Figure IV.3. Variation with frequency of the amplitude of the electric field produced in sea water by a linear current source of infinite length carrying an alternating current of amplitude 1000 A at a fixed perpendicular distance from the source. The electric field amplitudes for an arbitrary current can be derived from the values given above by multiplying by I/1000.

IV.4 Parametric Representation of the Fields

It is possible to write the amplitudes of the electric and magnetic fields given by Equations (IV.5) and (IV.6), in the parametric form, using the approach discussed in Section III.3. Normalizing the perpendicular distance of the field points from the sources by the skin depth, and generally following the rules in Section III.3, the electric and magnetic field expressions can be written in the following parametric form:

$$\left(\pi \sigma \delta^2 / I\right) |E_z| = \left(\ker_0^2 \left(\sqrt{2}\, a\right) + \mathrm{kei}_0^2 \left(\sqrt{2}\, a\right)\right)^{\frac{1}{2}}, \quad \text{(IV.7)}$$

and

$$\left(\sqrt{2}\pi\delta/\mu_0 I\right) |B_\phi| = \left(\ker_0'^2 \left(\sqrt{2}\, a\right) + \mathrm{kei}_0'^2 \left(\sqrt{2}\, a\right)\right)^{\frac{1}{2}}. \quad \text{(IV.8)}$$

The right hand sides of these two parametric expressions can be evaluated without difficulty and the data that are obtained are plotted in Figure IV.4. The curve with crossed circles gives the variation of the amplitude of the electric field in parametric form, as given by Equation (IV.7) and the other curve (dotted circles) gives the variation of the amplitude of the magnetic field in parametric form, as given by Equation (IV.8). The variable along the horizontal axis in these figures, $\sqrt{2}\, a$, is the argument of the Kelvin functions; it is essentially the perpendicular distance from the source in terms of skin depths. The two curves in Figure IV.4 are useful for rapid computation of the amplitudes of either the electric or magnetic fields produced in any arbitrary conducting medium of infinite extent by a linear current

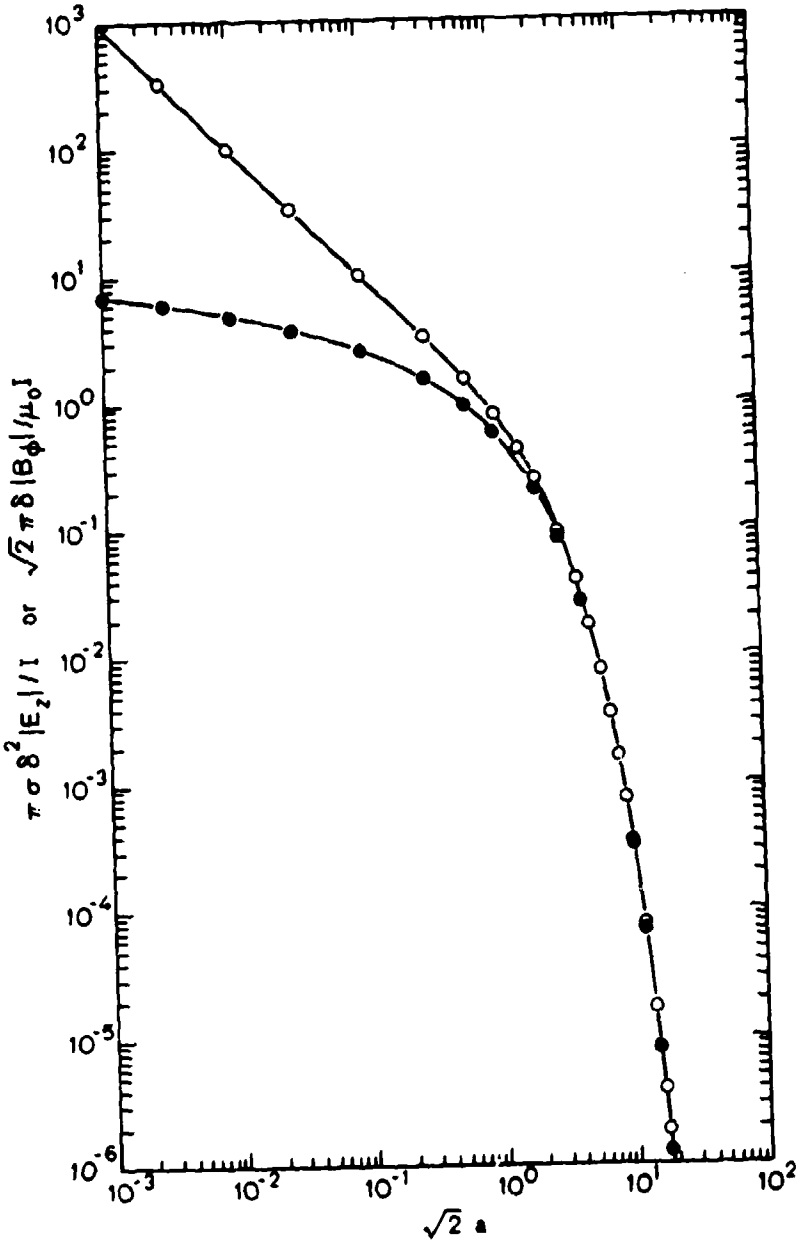

Figure IV.4. Variation with parametric distance $\sqrt{2}\,a$ (where $a = \rho_\delta = \rho/\delta$) of the parametric expressions for the amplitude of the electric field (crossed circles) and the magnetic field (dotted circles) produced in a conducting medium of infinite extent by a linear current source of infinite length carrying an alternating current of amplitude I.

source of infinite length over a very wide range of source currents and frequencies. For example, if the observation point is 100 m away (perpendicular distance) from the source and the source frequency is 1 Hz, we have $\sqrt{2}\,a \simeq 0.56$ and using Figure IV.4 we obtain approximately 1.0 and 1.6 for the parametric electric and magnetic field quantities given on the vertical axis of the figure. Knowing that $\delta = 251.6$ m for $f = 1$ Hz, $\sigma = 4$ S/m, and $\mu_o = 4\pi \times 10^{-7}$ H/m, and using $I = 10^3$A, we obtain $|E_z| \simeq 1.26$ mV/m and $|B_\phi| \simeq 1.80 \times 10^6$ pT. These particular values can be checked against the values of $|E_z|$ and $|B_\phi|$ plotted in Figures IV.1 and IV.2.

We have also plotted in Figure IV.5 the amplitude of the electric field in the alternate parametric form

$$(2\pi\sigma\rho^2/I)\,|E_z| = \left(\sqrt{2}\,a\right)^2 \left(\mathrm{ker}_o^2\left(\sqrt{2}\,a\right) + \mathrm{kei}_o^2\left(\sqrt{2}\,a\right)\right)^{1/2} . \quad (IV.9)$$

This is basically the same equation as Equation (IV.7), except that in Equation (IV.7) the left hand side is not a function of the perpendicular distance ρ and the left hand side of the above equation is not a function of frequency. In other words, the single curve shown in Figure IV.5 is a parametric form of the curves seen in Figure IV.3; it contains all their information on the variation of the amplitude of the electric field with perpendicular distance and source frequency, as well as much additional information of the field amplitudes at other distances. (If required, the field amplitudes can also be computed in other media than sea water.) The maximum value of the parametric electric field expression occurs for $\sqrt{2}\,a \simeq 2.17$. This is a useful result to

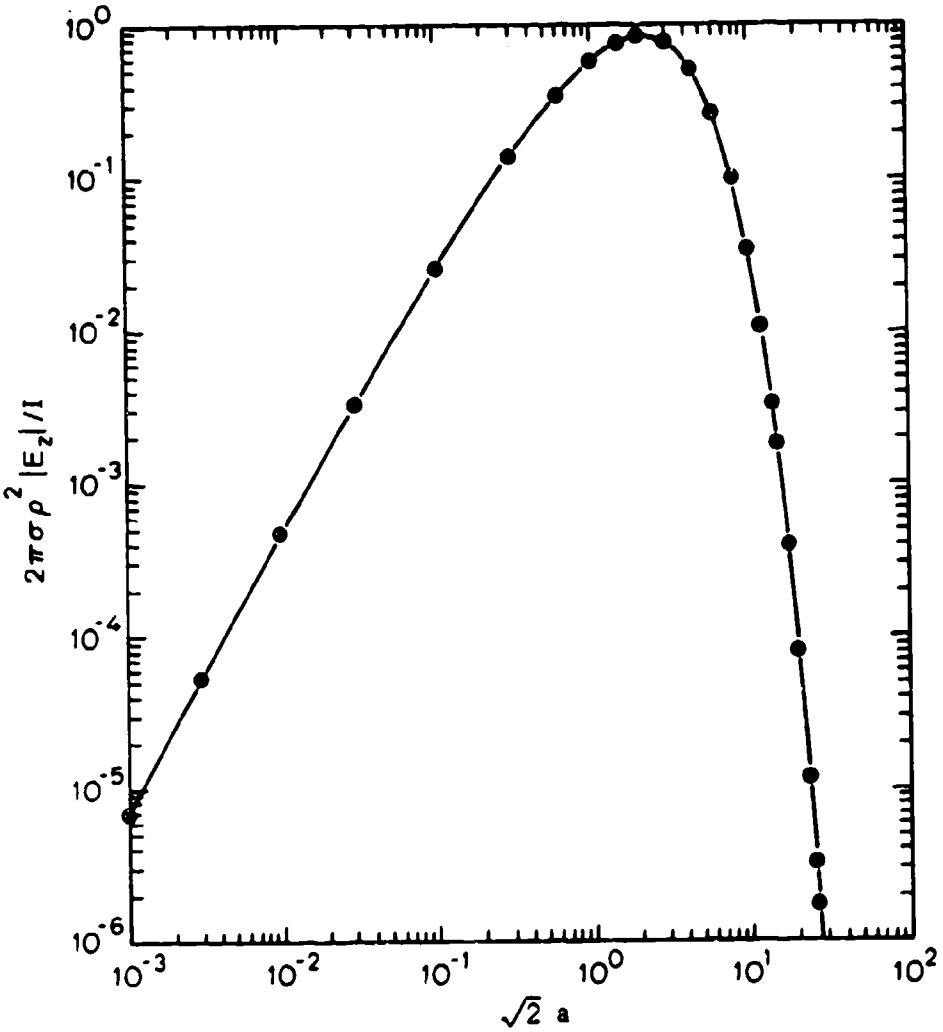

Figure IV.5. Variation with parametric distance $\sqrt{2}$ a (where a = ρ_δ = ρ/δ) of the parametric expression $2\pi\sigma\rho^2|E_z|/I$ for the amplitude of the electric field produced in a conducting medium of infinite extent by a linear current source of infinite length carrying an alternating current of amplitude I. Note that the maximum parametric amplitude (0.83) occurs for $\sqrt{2}$ a = 2.17.

remember, because it enables the optimum frequency of operation mentioned in the previous section and the corresponding maximum electric field to be computed. The procedure to obtain this information is as follows. First, knowing the location of the observation point (i.e., the perpendicular distance ρ), it is simple to obtain the frequency maximizing the amplitude of the electric field at that specific point from $\sqrt{2}\, a = \sqrt{2}\, \rho/\delta \simeq 2.17$. This is the frequency we will refer to as the optimum frequency. Next, the data in Figure IV.5 show that the maximum value of the parametric electric field expression $2\pi\sigma\rho^2 |E_z|/I$ is approximately 0.83, from which the actual value of the electric field amplitude can be computed.

V. LINEAR CURRENT SOURCE OF SEMI-INFINITE LENGTH

V.1 Derivation of the Electric and Magnetic Field Components

In the previous section we obtained expressions for the electric and magnetic fields produced by a linear current source of infinite length by letting ℓ_1 and ℓ_2 tend to minus infinity and infinity, respectively, in the expressions for the fields produced by a linear current source of finite length. In this section we concentrate our attention on the electric and magnetic fields surrounding the end of a linear current source immersed in a conducting medium of infinite extent, i.e., around an electrode of negligible size in the medium. We do this by letting just one end of the finite linear current source tend to infinity, thus producing a linear current source of semi-infinite length.

Starting with the finite source electric and magnetic fields expressions (Equations III.5 and III.12), letting ℓ_1 go to $-\infty$, and generally following a similar approach to the one used in Sections III and IV, we obtain the following three expressions for the non-zero fields in the conducting medium:

$$E_\rho = \frac{\rho I}{4\pi\sigma} \frac{e^{-\gamma r_2}}{r_2^3} (\gamma r_2 + 1), \qquad (V.1)$$

$$E_z = \frac{i\omega\mu I}{4\pi} \left[\left\{ \sinh^{-1} \frac{x_2}{a} - E_c [a, x_2] - \ker_o \left(\sqrt{2}\, a\right) \right\} \right.$$

$$\left. -i \left\{ E_s [a, x_2] + \mathrm{kei}_o \left(\sqrt{2}\, a\right) \right\} \right]$$

$$+ \frac{I}{4\pi\sigma} \frac{e^{-\gamma r_2}}{r_2^3} (\gamma r_2 + 1) (z - \ell_2), \qquad (V.2)$$

and

$$H_\phi = - \frac{\rho\beta^2 I}{4\pi} \left[\left\{ M_c[a, x_2] + M_s[a, x_2] + N_c[a, x_2] \right\} \right.$$

$$\left. + i \left\{ M_c[a, x_2] - M_s[a, x_2] - N_s[a, x_2] \right\} \right]$$

$$- \frac{\beta I}{2\sqrt{2}\,\pi} \left[\ker_0' \left(\sqrt{2}\, a\right) + i \mathrm{kei}_0' \left(\sqrt{2}\, a\right) \right] , \qquad (V.3)$$

where all the terms here are defined as in Section III.

When the observation point is on the axis of the semi-infinite wire (i.e., $\rho = 0$ and $z > \ell_2$), the above expressions simplify greatly to give

$$E_\rho = 0,$$

$$E_z = \frac{i\omega\mu I}{4\pi} \left[\left\{ \gamma_e + \frac{1}{2} \ln 2 + \ln x_2 - E_c[0, x_2] \right\} - i \left\{ E_s[0, x_2] - \frac{\pi}{4} \right\} \right]$$

$$+ \frac{\beta^2 I}{4\pi\sigma} \frac{e^{-(1+i)x_2}}{x_2^2} \left[(1+i)x_2 + 1 \right] , \qquad (V.4)$$

$$H_\phi = 0.$$

In these last equations γ_e is Euler's constant, which, to four significant figures, is given by $\gamma_e = 0.5772$. This constant is usually denoted by the symbol γ, but we have added the subscript e to distinguish it from the γ used here for the propagation constant. There is, of course, no relation between Euler's constant γ_e and the propagation constant γ.

V.2 Some Numerical Values

Figure V.1 shows contours of the maximum values reached by the two components of the electric field, E_ρ (solid line) and E_z (dashed line) around the end A of the semi-infinite source during one cycle of the current in the source (the amplitude of the current is assumed to be 1000 A). As can be seen, there are some regions in the figure where the ρ-component is larger than the z-component of the electric field, but for large distances the z-component becomes by far the largest component. This difference at large distances is caused by the overall inverse cube decline of the ρ-component with distance (see Equation V.1), in contrast to the z-component, which has only a partial inverse cube dependence on distance (Equation V.2). Note that as the point of observation begins to move towards the other end of the source, i.e., the end at infinity, the z-component contours become parallel to the source and the electric field values tend toward those produced by a linear current source of infinite length.

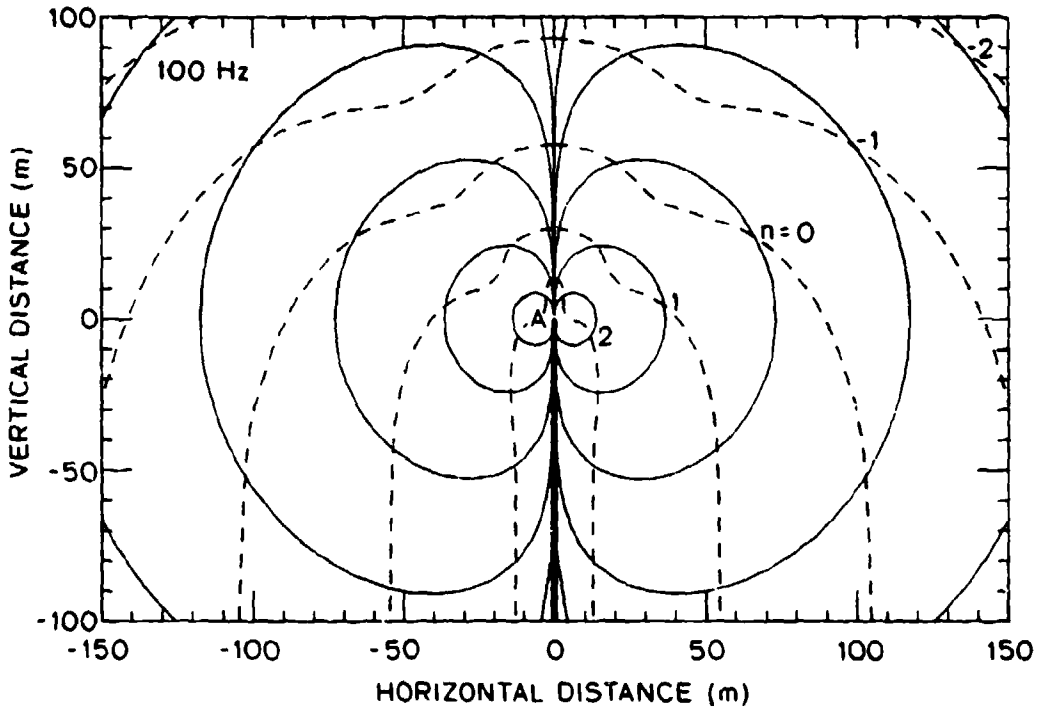

Figure V.1. Variation of the amplitudes of the ρ and z components of electric field, E_ρ and E_z, produced in sea water by a linear current source of semi-infinite length (extending from -∞ to A) and carrying an alternating current of amplitude 1000 A and frequency 100 Hz. The solid contours in this figure correspond to E_ρ, the dashed contours correspond to E_z, and the values of n shown for each contour give the numerical amplitude of the corresponding electric field in units of 10^n mV/m. Note that the field patterns are cylindrically symmetric about the axis defined by the source.

VI. LINEAR CURRENT SOURCE OF INFINITE LENGTH WITH A FINITE GAP

VI.1 Derivation of the Fields

In Section IV we investigated the electromagnetic field produced by an alternating current flowing in an insulated continuous linear current source of infinite length immersed in a homogeneous conducting medium of infinite extent. This system is distinguished by the fact that all the impressed current is effectively confined to the source. In other systems, for example linear current sources of finite or semi-infinite length, the impressed current also flows into the surrounding conducting medium from the ends of the wire. Suppose we now introduce a gap into our linear current source of infinite length so that the current in the source is forced to flow through the conducting medium over some finite distance. This system is equivalent to two semi-infinite linear current sources carrying the same current and aligned along the same axis but with a finite gap between them as shown in Figure VI.1(a).

We have already derived the electric and magnetic field expressions for a semi-infinite linear current source, so, using superposition, we can easily show that the fields produced by the system in Figure VI.1(a) are given by the following equations:

$$E_\rho = -\frac{\rho I}{4\pi\sigma}\left[\frac{e^{-\gamma r_2}}{r_2^3}(\gamma r_2 + 1) - \frac{e^{-\gamma r_1}}{r_1^3}(\gamma r_1 + 1)\right], \qquad (VI.1)$$

$$E_z = -\frac{i\omega\mu I}{2\pi}\left[\mathrm{ker}_0\left(\sqrt{2}\,a\right) + i\,\mathrm{kei}_0\left(\sqrt{2}\,a\right)\right]$$

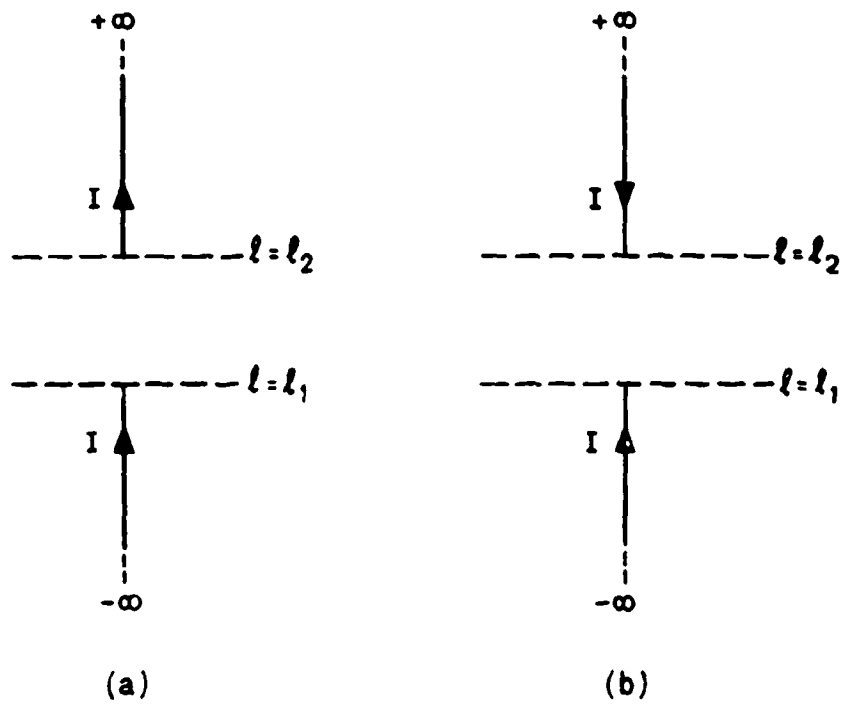

Figure VI.1. Sketches of the two linear current sources of infinite length with gaps that are considered in this work. In each case the gap extends from $\ell = \ell_1$ to $\ell = \ell_2$ and the amplitude of the current is the same in both the upper and lower semi-infinite segments. However, the directions of the current flow are different in the two systems. In case (a) the currents flowing in each segment are in the same direction, whereas in case (b) the currents are oppositely directed.

$$- \frac{i\omega\mu I}{4\pi} \left[\left\{ \sinh^{-1} \frac{x_2}{a} - \sinh^{-1} \frac{x_1}{a} - E_c[a, x_2] + E_c[a, x_1] \right\} \right.$$

$$\left. -i \left\{ E_s[a, x_2] - E_s[a, x_1] \right\} \right]$$

$$- \frac{I}{4\pi\sigma} \left[\frac{e^{-\gamma r_2}}{r_2^3} (\gamma r_2 + 1)(z - \ell_2) - \frac{e^{-\gamma r_1}}{r_1^3} (\gamma r_1 + 1)(z - \ell_1) \right] , \quad \text{(VI.2)}$$

and

$$H_\phi = - \frac{\beta I}{\sqrt{2}\,\pi} \left[\ker_0' \left(\sqrt{2}\, a \right) + i \, \mathrm{kei}_0' \left(\sqrt{2}\, a \right) \right]$$

$$+ \frac{\sigma\beta^2 I}{4\pi} \left[\left\{ M_c[a, x_2] - M_c[a, x_1] + M_s[a, x_2] - M_s[a, x_1] \right.\right.$$

$$\left. + N_c[a, x_2] - N_c[a, x_1] \right\}$$

$$+i \left\{ M_c[a, x_2] - M_c[a, x_1] - M_s[a, x_2] + M_s[a, x_1] \right.$$

$$\left.\left. - N_s[a, x_2] + N_s[a, x_1] \right\} \right] . \quad \text{(VI.3)}$$

It is interesting to note that, once again as a result of the principle of superposition, these expressions can be derived by subtracting the field expressions for a finite source of the same length as the gap from the field expressions for the continuous source of infinite length. Furthermore, if we are on the axis of the source and within the gap,

(i.e., $\rho = 0$ and $\ell_1 < z < \ell_2$), the field expressions become

$$E_\rho = 0,$$

$$E_z = \frac{i\omega\mu I}{4\pi}\left[2\gamma_e + \ln 2 + \ln(-x_1x_2) + E_c[0, x_2] - E_c[0, x_1] + i\left\{E_s[0, x_2] - E_s[0, x_1] + \frac{\pi}{2}\right\}\right] \qquad \text{(VI.4)}$$

$$+ \frac{\beta^2 I}{4\pi\sigma}\left[\frac{e^{-(1+i)x_1}}{x_1^2}\left((1+i)x_1+1\right) - \frac{e^{-(1+i)x_2}}{x_2^2}\left((1+i)x_2+1\right)\right],$$

$$H_\phi = 0.$$

A different version of this gap system can be obtained simply by reversing the direction of the current in one of the semi-infinite segments, so that the currents are oppositely directed in the two segments (Figure VI.1(b)). For this case, we can again make use of the semi-infinite wire expressions to derive the following electric and magnetic field expressions:

$$E_\rho = \frac{\rho I}{4\pi\sigma}\left[\frac{e^{-\gamma r_2}}{r_2^3}(\gamma r_2+1) + \frac{e^{-\gamma r_1}}{r_1^3}(\gamma r_1+1)\right], \qquad \text{(VI.5)}$$

$$E_z = \frac{i\omega\mu I}{4\pi}\left[\left\{\sinh^{-1}\frac{x_2}{a} + \sinh^{-1}\frac{x_1}{a} - E_c[a, x_2] - E_c[a, x_1]\right\}\right.$$

$$\left. -i\left\{E_s[a, x_2] + E_s[a, x_1]\right\}\right]$$

$$+ \frac{I}{4\pi\sigma}\left[\frac{e^{-\gamma r_2}}{r_2^3}(\gamma r_2+1)(z-\ell_2) + \frac{e^{-\gamma r_1}}{r_1^3}(\gamma r_1+1)(z-\ell_1)\right], \quad \text{(VI.6)}$$

and

$$H_\phi = -\frac{\rho\beta^2 I}{4\pi}\left[\left\{M_c[a, x_2] + M_c[a, x_1] + M_s[a, x_2] + M_s[a, x_1]\right.\right.$$

$$\left. + N_c[a, x_2] + N_c[a, x_1]\right\}$$

$$+ i\left\{M_c[a, x_2] + M_c[a, x_1] - M_s[a, x_2] - M_s[a, x_1]\right.$$

$$\left.\left. -N_s[a, x_2] - N_s[a, x_1]\right\}\right] . \quad \text{(VI.7)}$$

As we will see in the following section, the fields produced by the two gap systems have interesting differences in their properties.

VI.2 Numerical Results

As can be seen from the form of the field expressions VI.1 - VI.3 and VI.5 - VI.7, the spatial variations of the fields produced in and around the two finite gaps considered in this work are not simple. To illustrate these spatial variations, and to provide some representative numerical data, we make the comparatively simple fields produced by a

continuous infinite linear current source our reference and we compare the gap fields with these reference fields by computing ratios of the corresponding field quantities.

The first of these comparisons is made in Figure VI.2. where we have plotted the variation with perpendicular distance of the ratio of the amplitudes of the total electric field produced by (a) the infinite linear current source with a gap illustrated in Figure VI.1(a) (current flowing in the same direction in the two semi-infinite segments) and by (b) the continuous infinite linear current source. The current is everywhere assumed to be the same in the sources, the gap width is taken to be 100 m, and the variation with distance is taken along the perpendicular axis passing through the center of the gap. Because of the choice of this particular axis to show the distance variation, the ρ-component of the electric field produced by the gap system is zero at all the field points that are considered and the total electric field and E_z are equivalent for both sources.

The most interesting feature of the data in Figure VI.2 is the large ratio at small distances (i.e., $\rho < 1000$ m) for $f \leq 1$ Hz. At these frequencies the amplitude of the electric field in the vicinity of the gap can be substantially larger than the amplitude of the field that would be produced at the same locations by a continuous source carrying the same current. The increase begins to decline rapidly once a minimum perpendicular distance is exceeded. In Figure VI.2 this distance is approximately 50 m, which also happens to be the distance from the center of the gap to the near ends of the two semi-infinite segments.

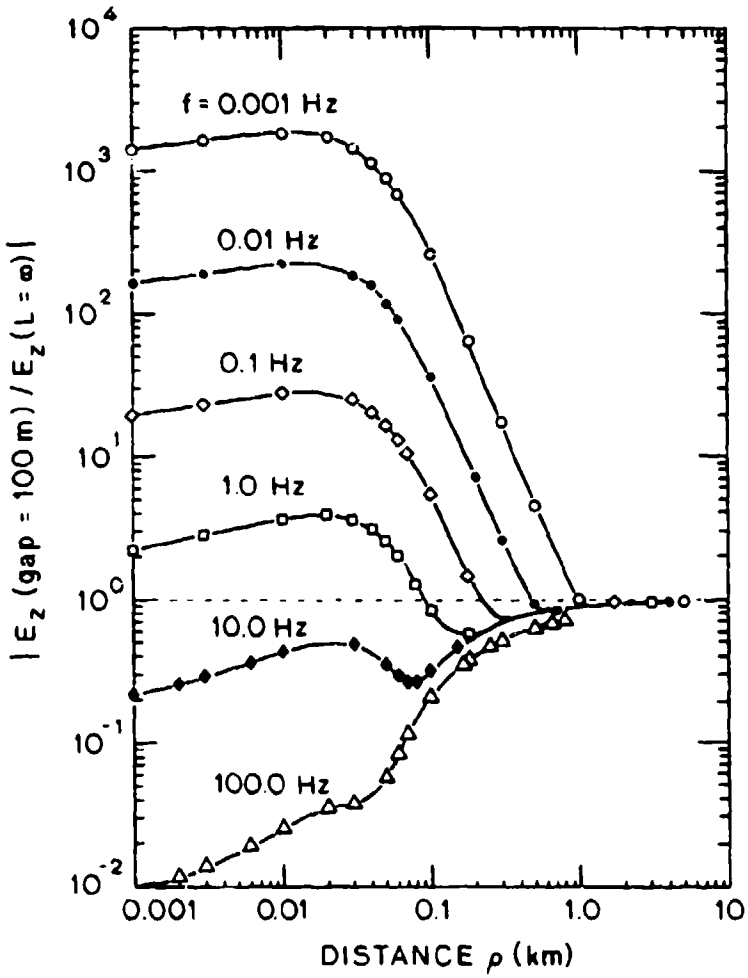

Figure VI.2. Variation with perpendicular distance of the ratio of the amplitudes of the z-components of the electric field produced (a) by a linear current source of infinite length with a finite gap (100 m), carrying current flowing in the same direction in each semi-infinite segment, and (b) by a continuous linear current source of infinite length. Both sources carry alternating currents of the same amplitude and frequency and the perpendicular axis along which the distance variation is shown passes through the center of the gap. The surrounding conducting medium (sea water, σ = 4 S/m) is assumed to be infinite in extent.

Beyond this minimum distance the ratio of the total field amplitudes rapidly approaches unity, no matter what frequency is involved, and at large distances the fields of the gap system approximate those produced by the continuous linear current source of infinite length.

A second comparison of the gap fields with the reference fields produced by a continuous source is made in Figure VI.3. In this figure the gap is the same size (100 m) as in the previous example, but the currents in the two semi-infinite segments are now taken in opposite directions. The figure therefore shows the variation with perpendicular distance of the ratio of the amplitudes of the total electric field produced by (a) the infinite linear current source with a gap illustrated in Figure IV. 1(b) (current flowing in opposite directions in the two semi-infinite segments) and by (b) the continuous infinite linear current source. As before, the amplitude of the current is everywhere considered to be the same in the sources and the variation with distance is taken along the perpendicular axis passing through the center of the gap. Again because of the choice of this particular axis to show the distance variation, the electric fields produced by the gap system have a distinguishing characteristic: the z-component of the electric field is zero at all the field points that are considered and the total electric field and E_ρ are equivalent. For the continuous source, the total electric field and E_z continue to be equivalent.

As was observed in the previous example, there is a region near the gap where the ratio is much larger than one for the lower frequencies ($f \leq 1$ Hz). This region extends out somewhat further from the gap than

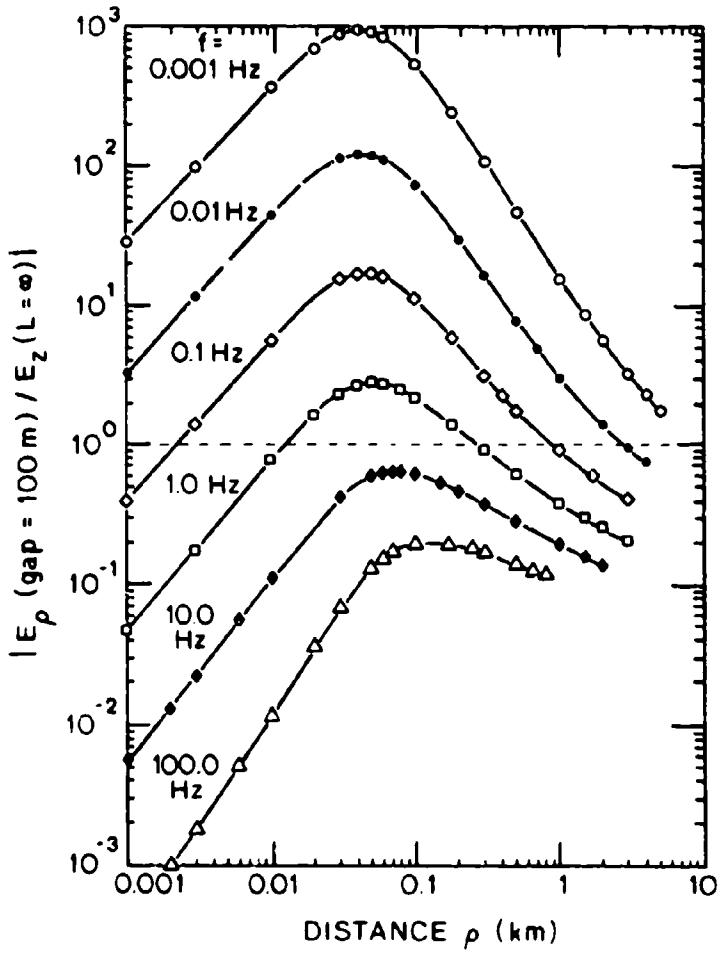

Fig. VI.3. Variation with perpendicular distance of the ratio of the amplitudes of (a) the ρ-component of the electric field produced by a linear length with a finite gap (100 m), with current flowing in opposite direction in each semi-infinite segment, and (b) the z-component of the electric field produced by a continuous linear current source of infinite length. Both sources carry alternating current of the same amplitude and frequency and the perpendicular axis along which the distance variation is shown passes through the center of the gap. The surrounding conducting medium (sea water, σ = 4 S/m) is assumed to be infinite in extent.

was observed before, which may be considered a positive characteristic of this particular gap system's electric field. On the other hand, at large distances the gap system's electric field decays more rapidly with distance than the electric field of the reference source and the ratio plotted in the figure becomes less than one.

Our third and final comparison of the electric fields produced by a gap system with the fields produced by other systems is made in Figure VI.4. In this case we have plotted the variations with frequency of the total electric fields produced at three different observation points, as follows: (1) an observation point at the center of the gap system (gap width - 100 m) illustrated in Figure VI.1(a); (2) an observation point 50 m away from the center of a linear current source (length = 100 m) and located on a perpendicular line through the center of the source; and (3) an observation point located 50 m away from a continuous linear current source of infinite length (our reference source). In all cases the amplitude of the current in the sources is 1000 A.

These final data show once again how the electric field of the reference source can be exceeded substantially by the fields produced either by gap systems or sources of finite length carrying the same total current when the frequencies and distances are small. However, as the field point distances increase and become large in terms of skin depths the fields produced by the continuous linear current source of infinite extent are at least as large as any of the other fields, and they may be substantially larger in some cases.

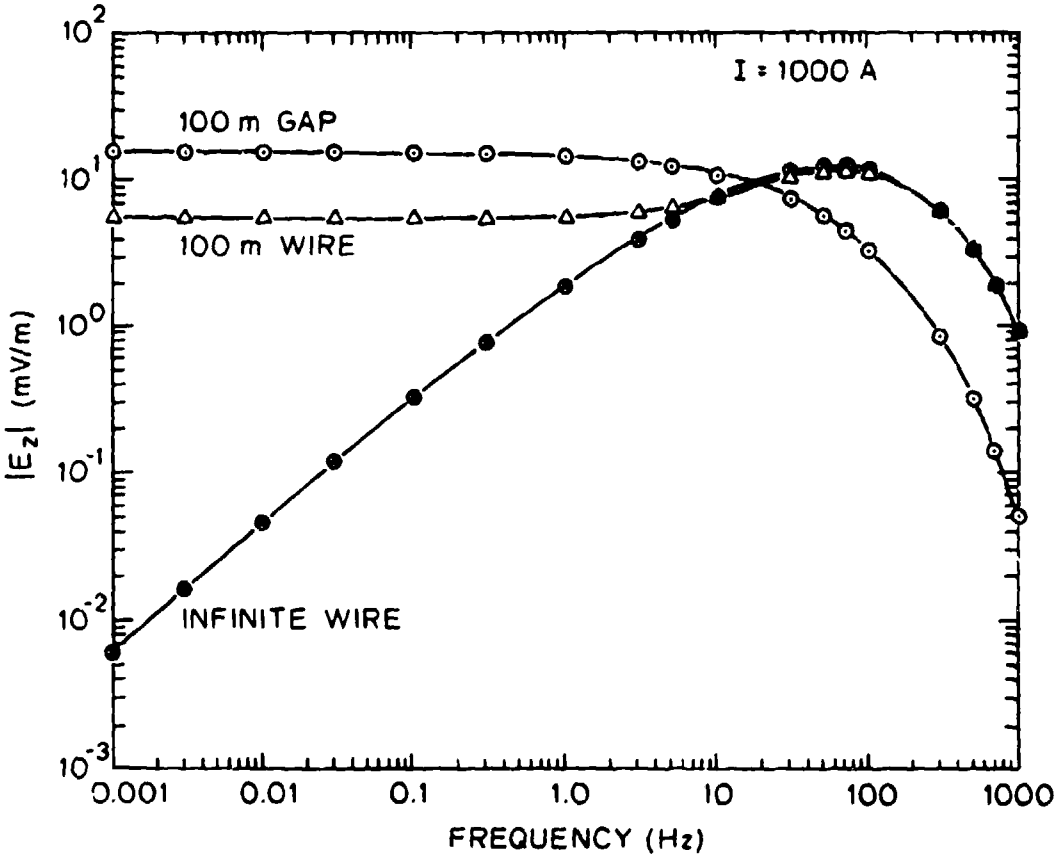

Figure VI.4. Comparison of the variations with frequency of the amplitudes of the z-component of the electric field for three cases: (1) $|E_z|$ produced by a linear current source of infinite length with a finite gap (100 m) carrying alternating current of amplitude 1000 A and with the observation point fixed at the center of the gap (dotted circles), (2) $|E_z|$ produced by a linear current source of finite length (100 m) carrying an alternating current of amplitude 1000 A, with the observation point fixed 50 m along a perpendicular line through the center of the source (triangles), (3) $|E_z|$ produced by a continuous linear current source of infinite length carrying an alternating 1000 A, with the observation point fixed 50 m away from the source (crossed circles). The surrounding conducting medium (sea water, σ = 4 S/m) is assumed to be infinite in extent. For each of the three cases the amplitude of the total electric field and $|E_z|$ are equivalent.

The electric and magnetic fields along the straight line joining the two ends of the gap, i.e., along the axis of the gap, have a simple vector form: the electric field has only a single component directed along the axis and the magnetic field is zero. Unfortunately, this simplicity does not carry over to the spatial variation of the electric field along the axis. Further, just off the axis the magnetic field has a non-zero azimuthal component, and this component also has a complicated spatial variation as the observation point moves along a line parallel to the axis. In general, both the axial electric field component and the off-axis magnetic field component are large near the two ends of the gap and they decrease as the observation point moves toward the center of the gap. The magnitude of the decrease depends in particular on the width of the gap and on the frequency: if the gap width is less than a skin depth, the decrease can be quite small; but if the width exceeds a skin depth, the decrease can be very large near the center of the gap. This behavior is well illustrated by the curve in Figure VI.4 showing the variation with frequency of the amplitude of the total electric field (i.e., the axial or z-component) at the center of a 100 m gap in sea water. It can be seen that as the frequency increases from 0.001 Hz there is little variation in the amplitude until the frequency reaches about 4 Hz (skin depth = 125.8 m), but by the time the frequency has reached 10 Hz (skin depth = 79.6 m) the amplitude has noticeably begun to decline.

VII. LINEAR CURRENT SOURCE OF INFINITE LENGTH WITH AN ELEMENTARY GAP

In the previous section we derived the fields produced by two semi-infinite linear current sources aligned along the same axis with a gap between them. If we now reduce the size of the gap until it becomes infinitesimal, we will obtain a linear current source of infinite length with an elementary gap in the middle.

Suppose the gap has an elementary length τ and that it is centered on the orgin. Starting from the Hertz vector expression for a current element source (Equation III.2) and integrating it with the right limits, we obtain the total Hertz vector due to the infinite length wire with an elementary gap:

$$\Pi_z = \frac{I}{4\pi\sigma} \int_{-\infty}^{-\tau/2} \frac{e^{-\gamma r}}{r} \, d\ell + \frac{I}{4\pi\sigma} \int_{+\tau/2}^{+\infty} \frac{e^{-\gamma r}}{r} \, d\ell \ , \qquad \text{(VII.1)}$$

which can also be written in the form

$$\Pi_z = \frac{I}{4\pi\sigma} \int_{-\infty}^{+\infty} \frac{e^{-\gamma r}}{r} \, d\ell - \frac{I}{4\pi\sigma} \int_{-\tau/2}^{+\tau/2} \frac{e^{-\gamma r}}{r} \, d\ell \ . \qquad \text{(VII.2)}$$

The two terms on the right of this last expression are easily recognized: the first term is the Hertz vector due to a continuous infinite linear current source and the second term is the Hertz vector due to a current element of elementary length τ.

Using Equations (II.5) and (II.6), the electric and magnetic fields for this system can be derived with little difficulty; they are given by the following expressions:

$$E_\rho = \frac{-I\tau \sin\theta \cos\theta}{4\pi\sigma r^3} (\gamma^2 r^2 + 3\gamma r + 3) e^{-\gamma r} , \qquad \text{(VII.3)}$$

$$E_z = \frac{-\gamma^2 I}{2\pi\sigma} K_0(\gamma\rho)$$

$$- \frac{I\tau}{4\pi\sigma r^3} \left[\cos^2\theta(\gamma^2 r^2 + 3\gamma r + 3) - (\gamma^2 r^2 + \gamma r + 1)\right] e^{-\gamma r}, \qquad \text{(VII.4)}$$

and

$$H_\phi = \frac{\gamma I}{2\pi} K_1(\gamma\rho) - \frac{I\tau \sin\theta}{4\pi r^2} (\gamma r + 1) e^{-\gamma r} , \qquad \text{(VII.5)}$$

where $\sin\theta = \rho/r$, $\cos\theta = z/r$, and $r = (\rho^2 + z^2)^{\frac{1}{2}}$. It is obvious, of course, that these field expressions are simply those for a continuous infinite wire less the corresponding expressions for a current element of length τ centered on the origin.

VIII. SUMMARY AND CONCLUSIONS

VIII.1 Summary

Starting with the theoretical work of Von Aulock [1948, 1953], Wait [1952, 1959, 1960], and Kraichman [1976], we have derived a number of new theoretical and numerical results for the ULF/ELF electromagnetic fields produced in a conducting medium of infinite extent by a variety of linear current sources. Many of the numerical results apply specifically to a sea water medium, since our work is oriented toward an undersea communication application, but the basic theory and some of the numerical data for the parametric expressions are given in a form that is independent of the specific conducting medium. The following is a list of the new results we have derived; in all cases the sources and observation points are taken to be in a conducting medium of infinite extent:

(1) We have greatly expanded the available numerical data on the electrical and magnetic field amplitudes produced by linear current sources of infinite length for frequencies in the range 0.001 - 1000 Hz. We have also introduced a parametric representation for these fields and, for any particular observation point, we have specified a technique for deriving the optimum frequency, i.e., the frequency for which the amplitude of the electric field is a maximum.

(2) We have extended the work of Wait [1952] on the electric fields produced by a linear current source of finite length by deriving an expression for the single magnetic field component (the azimuthal component) produced by such a source. We have also used a numerical integration

technique to obtain numerical values for the amplitudes of the electric and magnetic fields produced in sea water by representative finite sources.

(3) By extending one end of the finite source in (2) to infinity, we have derived new expressions for the electric and magnetic fields produced by a linear current source of semi-infinite length. Once again using numerical integration, representative numerical values for the two components of electric field have been obtained around the end (a "point electrode") of this semi-infinite source in sea water.

(4) By combining two of the semi-infinite sources described in (3), we have derived expressions for the electric and magnetic fields produced by a linear current source of infinite length containing a gap of finite size. Two versions of this source are considered: (a) currents of equal amplitudes flowing in the same directions in both semi-infinite segments, and (b) currents of equal amplitudes flowing in opposite directions in the two semi-infinite segments. Once again, representative numerical values have been computed for the amplitudes of the electric fields and the fields have been compared with those produced by an equivalent continuous source of infinite length.

(5) Finally, we have reduced the size of the finite gap in (4) until it is infinitesimally small and shown that the fields produced in the vicinity of the elementary gap are equivalent to the fields produced by a continuous linear current source of infinite length less the fields produced by an elementary current source at the location of the gap.

In general, we have made as few assumptions as possible in deriving

the above expressions and numerical data. The assumptions that are made can be summarized as follows. First, the displacement current is neglected. This is a very good assumption at all frequencies up to about 100 MHz if the surrounding medium is sea water. Second, we assume that the amplitude of the alternating current is the same throughout the various sources. At the ULF/ELF frequencies that are considered, this is equivalent to assuming that the current sources are insulated everywhere except at their ends. Third, we assume that the shortest distance between any observation point and the surface of the sources (which are taken to be circular in cross-section) is always much greater than the source radius. This assumption is discussed in greater detail in Appendix A. Finally, as we have pointed out many times, the conducting medium is always assumed to be infinite in extent.

VIII.2 Discussion

Our first objective in deriving the field expressions in Chapters III, V, and VI for sources of finite and semi-infinite length, and of infinite length with a gap of finite size, was to investigate the possible desirable characteristics of the fields near their open ends (i.e., point electrodes) for undersea communication at ULF/ELF frequencies. Assuming that this first part of our study gave positive results, our second objective was to derive enough theory and numerical data to provide the basis for the preliminary design of undersea communication arrays that would have the capability of producing measurable ULF/ELF signals throughout limited regions of the ocean without the cables pro-

ducing the signals necessarily being located in the regions. To a large extent our objectives have been achieved: comparatively large electric and, to a lesser extent, magnetic fields can be produced at ULF/ELF frequencies in the vicinity of the open ends of the sources considered in this work, and measurable ULF/ELF fields can be produced in and surrounding the region of a moderately large gap in an otherwise continuous current-carrying cable. However, it is important for us to point out that the same frequency versus range constraint applies in the case of the electromagnetic fields produced by undersea cables, with and without gaps, as is encountered in other methods of undersea communication involving electromagnetic signal propagation in sea water: large ranges can be achieved by using low frequencies, particularly low ULF frequencies, but because the rate of data transfer is directly proportional to the signal frequency, the rate of data transfer over the large ranges may be too small to be useful. As we will now show, this frequency versus range constraint effectively limits the use of discontinuous cable arrays to short range communication.

Comparing the ULF/ELF fields produced in sea water by cables of finite and semi-infinite length, and of infinite length with a gap, with the fields produced by a long continuous current-carrying cable (our linear current source of infinite length), our data show that at short distances from their open ends i.e., distances less than about 1 km, the discontinuous sources can produce greatly enhanced electric fields. We have not carried out a complete computation of all the field amplitudes that can be produced under all possible circumstances, but the available

data indicate that the increase is confined largely to frequencies in the ULF range and, within this range, it becomes larger as the frequency is decreased. At 0.001 Hz, for example, the increase of nearly 2000 times that is observed at a perpendicular distance of 10 m from the center of a 100 m gap in an otherwise continuous long current-carrying cable (Figure VI.2) is nearly 10 times larger than the increase at 0.01 Hz. In all the cases we have examined the increase begins to decline rapidly with distance once some limiting distance has been exceeded. For the two gap systems discussed in Chapter VI the limiting distance is of the same order as the width of the gap (100 m), a result that may be indicative of a general relation at the low ULF frequencies under consideration. It will be observed that the increase under discussion appears to be confined to the electric field, as may be seen by comparing the numerical data plotted in Figures III.9 and III.10 for the electric and magnetic fields produced by a cable of finite length. It is obvious from these and the other results we have derived that discontinuous sources have at best no advantage over the continuous linear source for field generation at distances much above 1 km and, at worst, they may produce much smaller fields than the continuous source for some geometries and frequencies. We conclude therefore that arrays of finite and/or semi-infinite cables, and continuous cable with gaps, can be used most advantageously for undersea communication only over short distances.

The possible situations where such communication could be used are not necessarily trivial. For example, the ULF/ELF electric fields around the gap between two point electrodes, or near a single point electrode,

could provide a low-data-rate, non-acoustic means of communication with an undersea or sea-floor receiver located beneath the hull of an electrode or cable/electrode equipped ship. At the short distances under consideration (distances $\leq$ 1 km) there is likely to be no difficulty providing communication with divers at frequencies in the lower part of the voice frequency range (50 - 3000 Hz); indeed, a commercial unit has been designed for an application of this kind [MacLeod, 1977]. As a final note on the possible communication applications of the discontinuous sources, we observe that long range is not always a desirable feature of a communication system, and under some circumstances the limited ranges for signal propagation that we have discussed here could be a decided advantage.

Turning now to the electromagnetic fields produced at large distances from the sources (distances of the order of 10 km, or greater), our data show, as we have commented above, that no discontinuous source produces larger fields than the long continuous current-carrying cable, and most of the sources produce smaller fields. Thus long continuous current-carrying cables appear to be the best choice if long distance undersea communication using the electromagnetic fields from cable sources is the goal. From the results given in Chapter IV, it can be seen that the maximum range that can be achieved with an alternating current of 1000 A with present electric and magnetic field sensors is of the order of 0.1 - 4 km for frequencies in the range 1000 - 1 Hz and of the order of 4 - 100 km for frequencies in the range 1 - [illegible] We assume that the cables are in a sea of [illegible] extent [illegible] lts; in

practice they will have to be located on the sea floor and sea-floor and sea-surface effects will influence the maximum ranges that can be achieved, but we would not expect the ranges to be extraordinarily different from those we have quoted unless the sea is electrically shallow and a significant up-over-and-down propagation mode exists [Fraser-Smith and Bubenik, 1979]. The maximum range that can be achieved at any frequency can be made larger either by increasing the amplitude of the current or by increasing the sensitivity of the sensors used to measure the electromagnetic fields. However, (1) our assumed 1000 A current is already substantial and a significant increase would entail large increases in power, and (2) the near-vertical slopes of most of the curves in Figures IV.1 and IV.2 as they approach the lower horizontal axes implies that even major increases in sensor sensitivity would only have a small effect on maximum range (even when no allowance is made for the presence of a background of natural noise). The range can always be increased by reducing the frequency, but the lowest frequencies considered in Figures IV.1 and IV.2 are already extraordinarily low by present undersea communication standards, which severely restricts the rate of data transfer, and there is the further disadvantage that the background noise increases rapidly with decreasing frequency throughout the ULF range. We conclude that maximum ranges of 1 - 10 km are likely to be the limit for a single long continuous cable and that undersea communication by means of the electromagnetic fields from ULF/ELF currents in undersea cables is necessarily restricted to special applications of limited range using either single long cables (transverse range 1 - 10 km) or arrays of long cables (trans-

verse ranges of a few tens to a few hundreds of kilometers, depending on the number of cables).

In Appendix D we consider two basic arrays of long cables: a series array, and a parallel array. Assuming once again that our infinite-sea ranges are comparable to those that would be computed for a real sea with both a sea surface and a sea floor, the results derived in the appendix indicate that a series array of 10 cables spaced 7.5 km apart and driven by a 1000 A current at 1 Hz could produce a measurable magnetic field at a distance of 1 km above the array (observation point in the sea) over a transverse distance of about 75 km and a longitudinal distance limited essentially to the length of the cables. The natural application of such arrays is to provide essential communication with undersea receivers throughout limited but important regions of the sea.

VIII.1 Suggestions for Further Work

An obvious extension of our work would be to include a sea floor and then, in addition, a sea surface in our theoretical formulation. Such an extension would involve a major new theoretical effort. A less obvious extension would be to consider the use of pulsed currents in the submerged cables, instead of the continuous alternating currents assumed in this work.

The above extensions are important, but perhaps the most important extensions that could be undertaken is a feasibility study to determine the practical utility of the proposed methods of undersea communication. We have indicated several different possible methods of using undersea

cables for communication, but we have necessarily omitted full consideration of their feasibility. Instead we have concentrated on making available the theoretical expressions and some of the numerical data that would be required in a feasibility study. We conclude by reiterating that most of the theoretical expressions and numerical data we have derived are new and as such they could well have unexpected implications for undersea communication. It would certainly be a departure from present practice to communicate up to a submerged receiver, instead of down to the receiver, and to have a signal-to-noise ratio that increases with depth in the sea. It is for these latter reasons, considered in relation to the growing importance of reliable undersea communication to the U.S. Navy, that the suggested feasibility study appears particularly appropriate at this time.

IX. REFERENCES

Butterworth, S., "The distribution of the magnetic field and return current round a submarine cable carrying alternating current. - Part 2," Phil. Trans. Roy. Soc. London, Ser. A, 224, 141, 1924.

Drysdale,C.V., "The distribution of the magnetic field and return current round a submarine cable carrying alternating current. - Part 1," Phil. Trans. Roy. Soc. London, Ser. A, 224, 95, 1924.

Dwight, H.B., Tables of Integrals and Other Mathematical Data, Fourth Edition, 336 pp., MacMillan, 1961.

Fraser-Smith, A.C., and D.M. Bubenik, "ULF/ELF electromagnetic fields generated above a sea of finite depth by a submerged vertically-directed harmonic magnetic dipole," Radio Science, 14, 59, 1979.

Kraichman, M.B., "Handbook of Electromagnetic Propagation in Conducting Media," Second Printing, U.S. Government Printing Office, Washington, D.C., 1976.

Lebedev, N.N., Special Functions and Their Applications, 308 pp., Dover, N.Y., 1972.

Lowell, H.H., Tables of the Bessel-Kelvin functions ber, bei, ker, kei, and their derivatives for the argument range 0(0.01)107.50, Tech. Rept. R-32, NASA, Lewis Res. Center. Cleveland, Ohio, 1959.

MacLeod, N., "Electric diver communication; Non-acoustic system can operate in noisy environments," Sea Technology, 18, 21, May 1977.

Panofsky, W.K.H., and M. Phillips, Classical Electricity and Magnetism, 494 pp., Addison-Wesley, Mass., 1962.

Scarborough, J.B., Numerical Mathematical Analysis, Sixth Edition, pp. 600, Johns Hopkins Press, Baltimore, 1966.

Staff, Computation Lab. of Harvard Univ., Tables of the Generalized Exponential-Integral Functions, 416 pp., Harvard Univ. Press, Cambridge, Mass., 1949.

Sunde, E.D., Earth Conduction Effects in Transmission Systems, 373 pp., Van Nostrand, N.Y., 1949.

Von Aulock, W., "Propagation of electromagnetic fields in sea water," Tech. Memo. No. 140, Dept. of the Navy, Bureau of Ships, Washington, D.C., May 1948.

Von Aulock, W., "The electromagnetic field of an infinite cable in sea water," Tech. Rept. No. 106, Dept. of the Navy, Bureau of Ships, Washington, D.C., 1 Sept. 1953.

Wait, J.R., "Electromagnetic fields of current-carrying wires in a conducting medium," Canadian J. Phys., 30, 512, 1952.

Wait, J.R., "Radiation from current distributions," pp. 167-200 in Electromagnetic Radiation from Cylindrical Structures, Pergamon, N.Y., 1959.

Wait, J.R., "Propagation of electromagnetic pulses in a homogeneous conducting earth," Applied Sci. Res., Sect. B, 8, 213, 1960.

Wright, C., "Leader Gear," pp. 177-184 in Proc. Symposium on Underwater Electromagnetic Phenomena, Ed. G.W. Wood, 216 pp., December 1953.

Young, A., and A. Kirk, Bessel Functions, Part IV; Kelvin Functions, Royal Soc. Math. Tables, Vol. 10, pp. 97, Cambridge Univ. Press, 1964.

APPENDIX A

THE INFINITELY-THIN LINEAR CURRENT SOURCE APPROXIMATION

In Section II we found that the inhomogeneous wave equation (Equation II.9) had a Hertz vector solution of the form

$$\underset{\sim}{\Pi} = \frac{1}{4\pi(\sigma + i\omega\varepsilon)} \int_V \frac{e^{-\gamma r}}{r} \underset{\sim}{J}\, dv \qquad (A.1)$$

in an unbounded homogeneous conducting medium. Here r is the distance between the volume element dv and the observation point P. Note that we use primed cylindrical coordinates (ρ', ϕ', z') for source point and unprimed coordinates (ρ, ϕ, z) for observation points. Our object in this Appendix is to derive a version of the above Hertz vector solution for a linear current source. As we will show, it is possible to obtain an approximate solution in which the volume integral is replaced by a line integral along the axis of the source.

Figure A.1 shows the cylindrical linear current source oriented in the z-direction and extending from $z' = \ell_1$ to $z' = \ell_2$. Its radius is ρ_c, and it carries current of density $J_z \exp(i\omega t)$. From Equation (A.1), the Hertz vector for this case has only a z-component which can be written as

$$\Pi_z = \frac{1}{4\pi(\sigma + i\omega\varepsilon)} \int_{\ell_1}^{\ell_2} \int_0^{2\pi} \int_0^{\rho_c} \frac{e^{-\gamma r}}{r} J_z(\rho', \phi', z')\rho' d\rho' d\phi' dz' , \qquad (A.2)$$

where

$$r = [\rho^2 + \rho'^2 - 2\rho\rho' \cos(\phi - \phi') + (z - z')^2]^{\frac{1}{2}} . \qquad (A.3)$$

We will assume that the current density J_z is a function of z' only. We will then consider the following two conditions:

(i) $\rho >> \rho'$ for all ρ', so that $(\rho \pm \rho') \approx \rho$.

(ii) $(z-z')^2 >> (\rho+\rho')^2$, so that $(\rho \pm \rho')^2 + (z-z')^2 \approx (z-z')^2$.

These conditions have the following physical significance. First, condition (i) implies that the ρ-component of the observation point must be much larger than the radius of the cylindrical linear current source. Second, condition (ii) implies that the shortest vertical distance from the observation point to the cylindrical linear current source is much larger than both the ρ-component of the observation point and the radius of the source. Note that the two conditions do not necessarily apply simultaneously.

If the first condition is true, it follows that $r \approx [\rho^2 + (z-z')^2]^{\frac{1}{2}}$. If the second condition is true, it follows that $r \approx |z-z'|$. If any of these conditions is true, the distance r is no longer a function of ρ' and ϕ' and the Hertz vector can be rewritten as

$$\Pi_z = \frac{1}{4\pi(\sigma+i\omega\varepsilon)} \int_{\ell_1}^{\ell_2} \frac{e^{-\gamma r}}{r} J_z(z') \int_0^{2\pi} \int_0^{\ell_c} \rho' d\rho' d\phi' dz' , \quad (A.4)$$

where the two integrals on the right hand side give $\pi\rho_c^2$. Since $\pi\rho_c^2 J_z(z') = I_z(z')$, it follows that

$$\Pi_z \approx \frac{1}{4\pi(\sigma+i\omega\varepsilon)} \int_{\ell_1}^{\ell_2} \frac{e^{-\gamma r}}{r} I_z(z') \, dz . \quad (A.5)$$

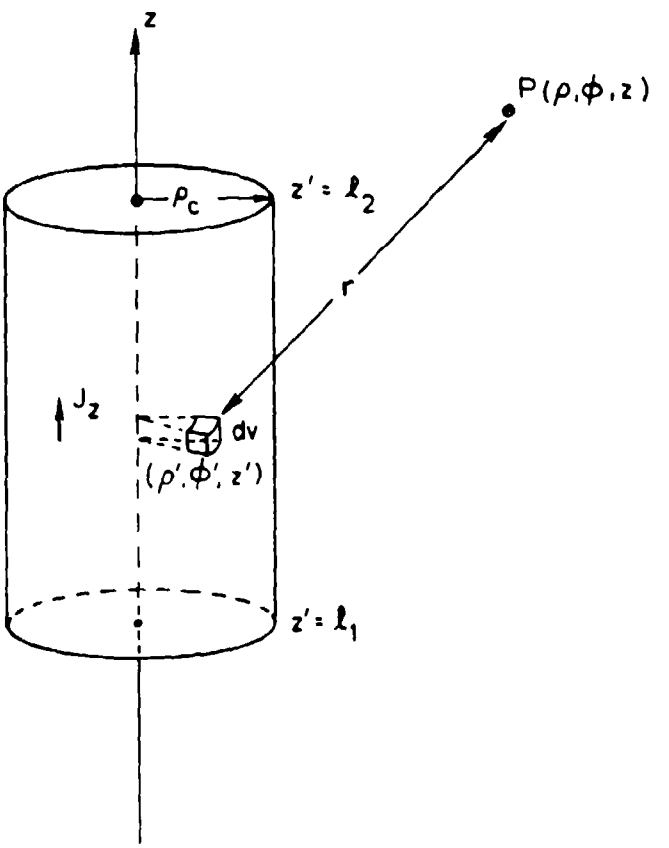

Figure A.1. Cylindrical antenna of finite length ($\ell_2 - \ell_1$) and finite cross-section (radius ρ_c) carrying a current with a uniform density J_z. A small volume element dv of the antenna is also shown in the figure.

In our derivations, we have always used Equation (A.5) for the Hertz vector. This means that all our field expressions are valid as long as one of the above conditions (i) and (ii) are satisfied, i.e., as long as the shortest distance from the observation point to the cylindrical linear current source is much larger than the radius of the cylindrical linear current source itself. In other words, we assume that the linear current source is infinitely thin.

APPENDIX B

INTRODUCTION OF THE KELVIN FUNCTIONS

In Section IV, Equation (IV.2), we have an integral of the form

$$I_1 = \int_0^\infty \frac{e^{-(1+i)u}}{u}\, dx \,, \tag{B.1}$$

where $u = (a^2 + x^2)^{\frac{1}{2}}$, which we want to express in terms of known functions.

This integral can also be written as

$$I_1 = \int_a^\infty \frac{e^{-(1+i)u}}{\sqrt{u^2-a^2}}\, du \,. \tag{B.2}$$

Defining $u = at$, this integral can be rewritten as

$$I_1 = \int_1^\infty \frac{e^{-(1+i)at}}{\sqrt{t^2-1}}\, dt \,. \tag{B.3}$$

From Lebedev [1972; see p. 119], we have the following integral expression for the n-th order modified Bessel function of the second kind:

$$K_n(z) = \frac{\sqrt{\pi}}{\Gamma(n+\frac{1}{2})} \left(\frac{z}{2}\right)^n \int_1^\infty e^{-zt} \left(t^2-1\right)^{n-\frac{1}{2}}\, dt \tag{B.4}$$

provided Re $z > 0$ and Re $n > -\frac{1}{2}$. Here, Γ is the Gamma Function defined as

$$\Gamma(n) = \int_0^\infty y^{n-1} e^{-y} dy. \tag{B.5}$$

Choosing $n = 0$ and knowing that $\Gamma(\frac{1}{2}) = \sqrt{\pi}$, Equation (B.4) becomes

$$K_0(z) = \int_1^\infty \frac{e^{-zt}}{\sqrt{t^2-1}}\, dt. \tag{B.6}$$

Substituting $z = a(1+i)$ in Equation (B.6) and comparing it with Equation (B.3), we obtain

$$K_0\left(a(1+i)\right) = I_1. \tag{B.7}$$

In other words, the integral I_1 is a zero-th order modified Bessel function of the second kind of complex argument. Knowing this fact, we can now proceed to write I_1 in terms of known functions.

Since $\gamma = (1+i)\beta$ and $a = \beta\rho$, we have

$$K_0\left(a(1+i)\right) = K_0(\gamma\rho) \tag{B.8}$$

and from these relations it follows that

$$I_1 = K_0(\gamma\rho) = \int_0^\infty \frac{e^{-(1+i)u}}{u}\, dx. \tag{B.9}$$

We also know from Dwight [1961] that

$$i^{-n} K_n\left(\alpha \sqrt{i}\right) = \ker_n \alpha + i \, \mathrm{kei}_n \alpha , \qquad (B.10)$$

where $\ker_n \alpha$ and $\mathrm{kei}_n \alpha$ are Kelvin functions of the second kind of order n [Young and Kirk, 1964]. The left hand side of Equation (B.10) can also be written as

$$K_n\left(\alpha \sqrt{i}\right) = K_n\left(\alpha(1+i)/\sqrt{2}\right). \qquad (B.11)$$

Letting n = 0 and following equations (B.8) - (B.11), we have

$$I_1 = K_0(\gamma\rho) = \ker_0\left(\sqrt{2}\, a\right) + i \, \mathrm{kei}_0\left(\sqrt{2}\, a\right) . \qquad (B.12)$$

We have now expressed the integral I_1 in terms of known Kelvin functions. If we decompose I_1 in equation (B.9) into its real and imaginary parts, we obtain

$$I_1 = K_0(\gamma\rho) = \int_0^\infty \frac{e^{-u}\cos u}{u}\, dx - i \int_0^\infty \frac{e^{-u}\sin u}{u}\, dx , \qquad (B.13)$$

then, comparing equations (B.12) and (B.13), it follows that

$$\begin{aligned} \ker_0\left(\sqrt{2}\, a\right) &= \int_0^\infty \frac{e^{-u}\cos u}{u}\, dx , \\ \mathrm{kei}_0\left(\sqrt{2}\, a\right) &= -\int_0^\infty \frac{e^{-u}\sin u}{u}\, dx . \end{aligned} \qquad (B.14)$$

If we let the upper limits of the integrals given by Equation (III.8) go to infinity and compare the results with the integrals in Equation (B.14), we can write

$$\ker_0 (\sqrt{2}\, a) = \int_0^\infty \frac{1}{u}\, dx - E_c [a, \infty] ,$$

$$\text{kei}_0 (\sqrt{2}\, a) = - E_s [a, \infty] . \tag{B.15}$$

Similarly, if we also let the upper limits of the integrals given by Equation (III.16) go to infinity and compare the results with the derivatives of the Kelvin functions given by Equation (B.14), we obtain

$$\ker_0' (\sqrt{2}\, a) = \frac{-a}{\sqrt{2}} \left(M_c[a, \infty] + M_s[a, \infty] + N_c[a, \infty] \right) ,$$

$$\text{kei}_0' (\sqrt{2}\, a) = \frac{-a}{\sqrt{2}} \left(M_c[a, \infty] - M_s[a, \infty] - N_s[a, \infty] \right) . \tag{B.16}$$

Since we also know that

$$\ker_1 (\sqrt{2}\, a) = \frac{1}{\sqrt{2}} \left(\ker_0' (\sqrt{2}\, a) - \text{kei}_0' (\sqrt{2}\, a) \right) ,$$

$$\text{kei}_1 (\sqrt{2}\, a) = \frac{1}{\sqrt{2}} \left(\ker_0' (\sqrt{2}\, a) + \text{kei}_0' (\sqrt{2}\, a) \right) , \tag{B.17}$$

we can substitute Equations (B.16) into Equations (B.17) and obtain

$$\ker_1 (\sqrt{2}\, a) = \frac{-a}{2} \left(2M_s [a, \infty] + N_c [a, \infty] + N_s [a, \infty] \right) ,$$

$$\text{kei}_1 (\sqrt{2}\, a) = \frac{-a}{2} \left(2M_c [a, \infty] + N_c [a, \infty] - N_s [a, \infty] \right) . \tag{B.18}$$

APPENDIX C

FIELDS PRODUCED BY A DC CURRENT

In this appendix we summarize the electric and magnetic field expressions for dc currents flowing in linear current sources of infinitesimal, finite, semi-infinite, and infinite length.

1. Current Element Source

The fields produced by linear current element of length $d\ell$ and carrying a dc current I are given by

$$E_\rho = \frac{3Id\ell \sin\theta \cos\theta}{4\pi\sigma r^3} ,$$

$$E_z = \frac{Id\ell}{4\pi\sigma r^3} (3\cos^2\theta - 1) , \qquad (C.1)$$

$$H_\phi = \frac{Id\ell \sin\theta}{4\pi r^2} ,$$

and

$$E_\phi = H_\rho = H_z = 0 .$$

2. Linear Current Source of Finite Length

The fields due to a linear current source of finite length carrying a dc current I and extending from ℓ_1 to ℓ_2 are

$$E_\rho = \frac{\rho I}{4\pi\sigma}\left[\frac{1}{r_2^3} - \frac{1}{r_1^3}\right] ,$$

$$E_z = \frac{I}{4\pi\sigma}\left[\frac{z-\ell_2}{r_2^3} - \frac{z-\ell_1}{r_1^3}\right] , \qquad (C.2)$$

and

$$H_\phi = \frac{I}{4\pi\rho}\left[\frac{z-\ell_1}{r_1} - \frac{z-\ell_2}{r_2}\right] .$$

with $E_\phi = H_\rho = H_z = 0$.

Now consider a perpendicular line passing through the center of the source. Along this line, $E_\rho = 0$ and we have

$$E_z = \frac{-IL}{4\pi\sigma r^3} ,$$

and

$$H_\phi = \frac{IL}{4\pi\rho r} ,$$

where $L = \ell_2 - \ell_1$ is the length of the source.

If we normalize all the distances to the length L of the source, we obtain

$$L^2 E_z = \frac{-I}{4\pi\sigma r_L^3} ,$$

and (C.3)

$$LH_\phi = \frac{I}{4\pi\rho_L r_L} ,$$

where $\rho_L = \rho/L$ and $r_L = r/L$.

In Figure C.1, we have plotted the variation of the magnitude of the normalized E_z field (i.e., $E_z L^2$) with normalized distance ρ_L.

3. Linear Current Source of Infinite Length

Given a linear current source of infinite length carrying a dc current I, all the field components are zero except for the magnetic field component H_ϕ, where

$$H_\phi = \frac{I}{2\pi\rho} \quad . \tag{C.4}$$

4. Linear Current Source of Semi-Infinite Length

In the case of a semi-infinite linear current source extending from $-\infty$ to ℓ_2 and carrying a dc current I, we have

$$E_\rho = \frac{\rho I}{4\pi\sigma r_2^3} \quad ,$$

$$E_z = \frac{I}{4\pi\sigma r_2^3} \ (z-\ell_2) \ , \tag{C.5}$$

$$H_\phi = \frac{I}{4\pi\rho} \left[1 - \frac{z-\ell_2}{r_2} \right] \ ,$$

and

$$E_\phi = H_\rho = H_z = 0 \ .$$

5. Linear Current Source of Infinite Length with a Finite Gap

Assuming the direction of current flow is the same in the two segments of the source (Figure VI.1(a)), we have

$$E_\rho = \frac{\rho I}{4\pi\sigma}\left[\frac{1}{r_1^3} - \frac{1}{r_2^3}\right],$$

$$E_z = \frac{I}{4\pi\sigma}\left[\frac{z-\ell_1}{r_1^3} - \frac{z-\ell_2}{r_2^3}\right], \qquad (C.6)$$

and

$$H_\phi = \frac{I}{4\pi\rho}\left[\frac{z-\ell_2}{r_2} - \frac{z-\ell_1}{r_1}\right].$$

Again, $E_\phi = H_\rho = H_z = 0$.

These equations are the negative of Equations (C.2), which means that in the dc case, the gap system produces fields of the same magnitude but pointing in opposite directions compared with a linear current source of finite length carrying the same current I as flows through the gap and occupying the same position as the gap. Thus if the gap length is L (i.e., $\ell_2-\ell_1 = L$), the plot of the magnitude of the electric field along the perpendicular line passing through the center of the gap will be exactly the same as the one shown for a linear current source of finite length in Figure C.1.

If the currents in the two semi-infinite segments are directed towards each other (See Figure VI.1(b)), instead of in the same direction as above, the electric and magnetic field expressions become

$$E_\rho = \frac{\rho I}{4\pi\sigma}\left[\frac{1}{r_1^3} + \frac{1}{r_2^3}\right],$$

$$E_z = \frac{I}{4\pi\sigma}\left[\frac{z-\ell_1}{r_1^3} + \frac{z-\ell_2}{r_2^3}\right], \qquad (C.7)$$

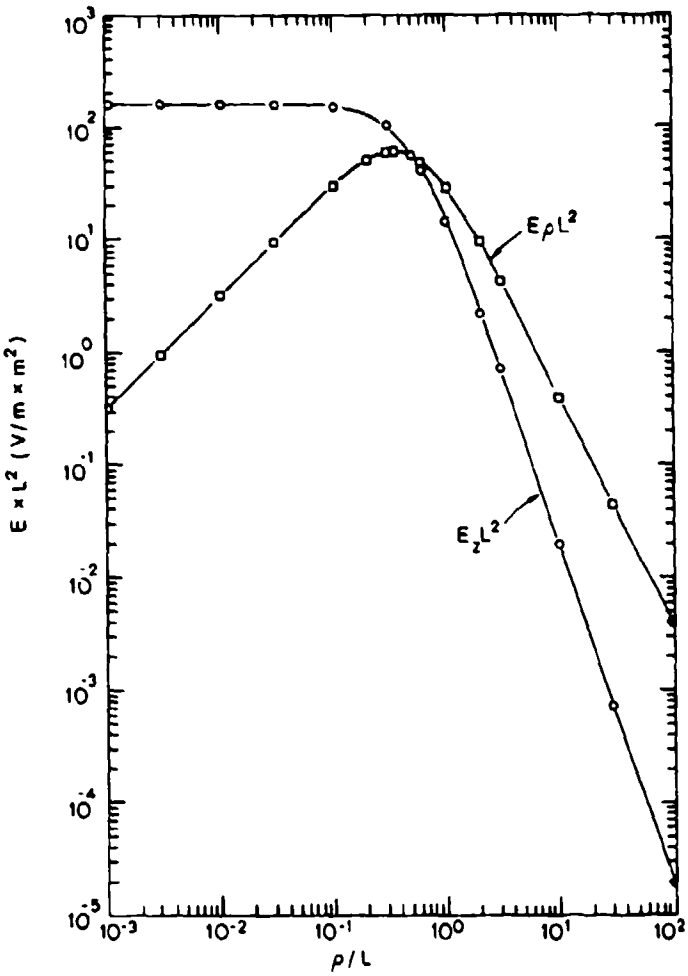

Figure C.1. Variation with normalized perpendicular distance ρ/L of the total electrical fields produced in sea water by linear current sources carrying dc currents of 1000 A. One curve (circles) applies to both a linear current source of finite length L and to a linear current source of infinite length having a finite gap of length L with the current flowing in the same direction in each semi-infinite segment. The other curve (squares) corresponds to a linear current source of infinite length having a finite gap of length L with the current flowing in opposite directions in each semi-infinite segment. The perpendicular axis along which the distance variations are shown passes through the central point of each source.

and

$$H_\phi = \frac{-I}{4\pi\rho}\left[\frac{z-\ell_1}{r_1} + \frac{z-\ell_2}{r_2}\right] .$$

If we now restrict ourselves to the fields produced along the perpendicular line passing through the center of the gap of finite length L and normalize all the distances with L, we obtain

$$L^2 E_\rho = \frac{\rho_L I}{2\pi\sigma r_L^3} ,$$

$$E_z = 0 , \qquad (C.8)$$

$$H_\phi = 0 .$$

The variation of the magnitude of the normalized E_ρ field (i.e., $E_\rho L^2$) with normalized distance ρ_L for this case is plotted in Figure C.1.

If we now compare the electric field variations shown in Figure C.1, we find that the electric field produced by the gap system with opposite current flow shown in Figure VI.1(b) declines less rapidly with distance (once ρ exceeds L/2) than the electric field produced either by the gap system with currents flowing in the same direction in each semi-infinite segment, as shown in Figure VI.1(a), or by the linear current source of length L. The respective slopes of the two curves are -20 dB/decade and -30 dB/decade at large distance.

APPENDIX D

FIELDS PRODUCED BY ARRAYS OF LONG CABLES SUBMERGED IN A CONDUCTING MEDIUM OF INFINITE EXTENT

As discussed in Chapter VIII, the data displayed in the figures in Chapter IV suggest that a single submerged cable cannot produce electric or magnetic fields with the right frequency/amplitude characteristics for successful undersea communication once the range exceeds some value that will typically lie in the range 1 - 10 km (the actual value will depend on a number of practical details; some of the most important of these details are the frequency, the amplitude of the current in the cable, the amplitude of the signal, the range, the background noise level, and the sensitivity of the receivers). However, there appears to be no reason why the range cannot be extended more or less indefinitely, in principle, by the use of arrays of long cables. The problem of range is then converted to a problem of cost and of power availability. In this appendix we briefly consider some of the requirements for these arrays and the ranges that might be achieved.

As a first example of an array of long cables, consider the configuration of cables (length L) shown in the top panel of Figure D.1. We will refer to this configuration as a series array, and we will assume that L is so large that we can treat each cable in the array as a linear current source of infinite extent and thus compute the electric and magnetic fields they produce from the expressions and data given in Chapter IV. We also assume that the spacing s, although small compared with L, is large enough for each cable to be treated as being independent of its

neighbors. A second example of an array of long cables, a parallel array, is shown in the bottom panel of Figure D.1; we will make the same assumptions for this array as those we have just detailed for the series array. We will suppose that the origin of a 3-dimensional cartesian coordinate system (x,y,z) is located at the center of each array and that the planes of the two arrays correspond to the x,y planes of the coordinate systems, with the y axis taken parallel to the cables as shown in the figure.

Cross-sections of the two arrays, taken along the x-axis in Figure D.1, are shown in Figure D.2. Here the cables are designated C_{-n}, C_{-n+1}, ... C_{-1}, C_{+1}, ... C_n according to their position relative to the origin of the coordinate system. Considering the series array first, it is easily seen that the total electric field at an observation point located at a height h above the origin, i.e., at the point (0,0,h) is always zero. However, the magnetic fields produced by each cable add up vectorially and give a total magnetic field that is directed along the z-axis. The first two vector contributions to this field, the magnetic fields $\underset{\sim}{B}_{+1}$ and $\underset{\sim}{B}_{-1}$ produced by the two nearest cables, are shown in the figure. The electric and magnetic fields produced by the parallel array differ substantially from those produced by the series array. Considering the fields produced at the point (0,0,h) once again, we find that the parallel array does produce an electric field, unlike the series array, and the field is directed along the y axis. Further, instead of being directed along the z-axis, i.e., in a direction perpendicular to the plane of the array, the magnetic field produced by the parallel array is

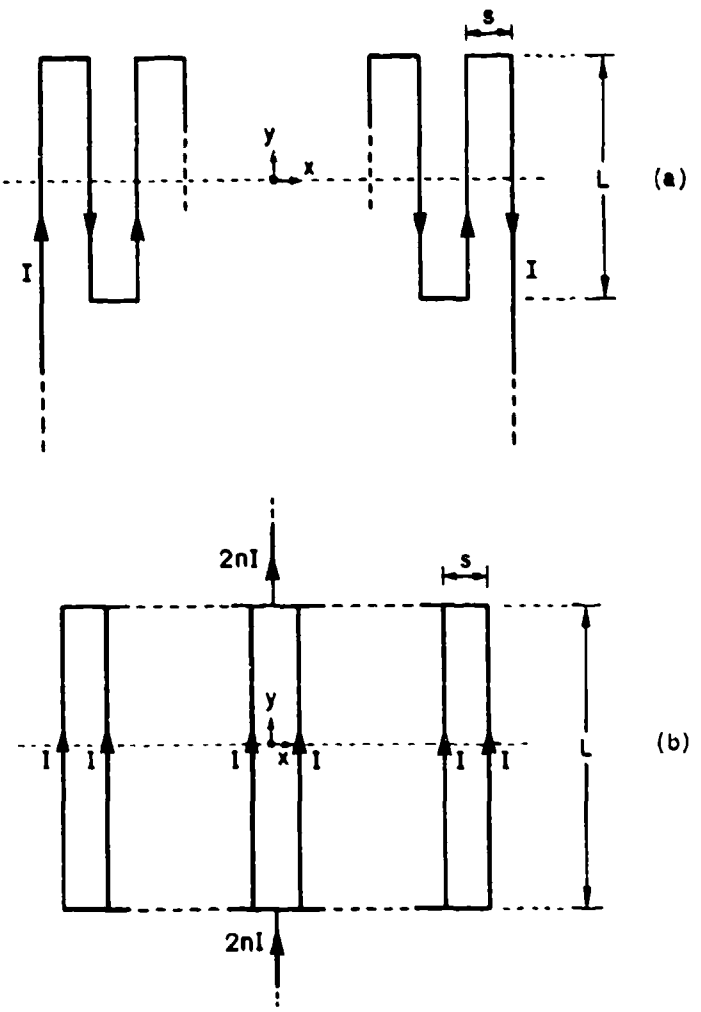

Figure D.1. Two different arrays of parallel long cables (length = L, spacing = s; s<<L) lying in the same plane and all carrying the same current I. In the top panel (a) we show a series array, where the current in a particular cable flows in the opposite direction to the current in the adjacent cables. In the bottom panel (b) we show a parallel array, where the current in all the cables flows in the same direction. Note that the total current flowing through the series array is I, whereas the total current flowing through the parallel array is 2nI, where 2n (n = 1,2,3...) is the number of cables in each array.

directed along the x-axis, i.e., in a direction parallel to the plane of the array. These various properties of the fields do not apply generally, but they illustrate the large differences that can occur in the fields produced by the two arrays.

In considering arrays, our primary interest is to produce measurable electric and/or magnetic fields throughout as large a volume of the sea as possible, with the least number of cables. Or, since the sea is comparatively limited in depth compared with horizontal extent, we wish to produce measurable fields throughout the sea over as large an area as possible. Clearly the cables in the arrays (which we now assume are located on the sea floor, although this is not a necessary condition for the use of the arrays we have been considering) must be spaced far apart, with the actual spacing being determined by the fields produced at points midway between the cables, where the attenuation of the fields is relatively the strongest and where the field amplitudes are in most cases a minimum for a given height h above the plane of the arrays. To illustrate the amplitudes of the fields that can be produced, we have taken the series array shown in Figure D.1(a) and D.2(a) and computed the variation of the amplitude of the total magnetic field with height h along two axes perpendicular to the plane of the array: the z-axis, which passes through a point (the origin) located midway between two cables, and an axis passing through one of the cables. Because our interest is in the fields produced by an array of widely spaced cables, we assume that the distance s between the cables is 30 skin depths, which means that we can reasonably neglect the fields produced along our two chosen

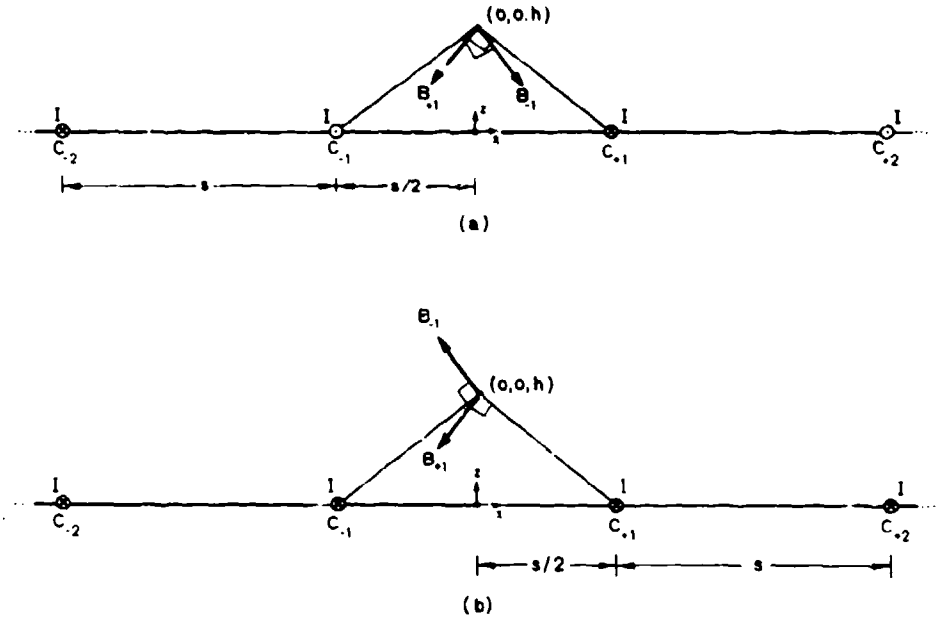

Figure D.2. Cross-sectional views of the two arrays of long cables shown in Figure D.1. At top is the series array, where the direction of the current in any cable is opposite to the direction of the current in adjacent cables; at bottom is the parallel array, where the direction of the current is the same in all cables. The magnetic fields B_{-1} and B_{+1} produced at the observation point (o,o,h) by the two cables C_{-1} and C_{+1} are shown for each array.

axes by all the cables in the array except for the one or two cables nearest to the axes. Equation (IV.6) is used to obtain the magnetic fields produced by these cables.

Figure D.3 shows the results of the computations. The data are presented in parametric form, so that they apply at any ULF/ELF frequency, and it is immediately apparent by comparing the two curves in the figure that the total magnetic field produced along the axis passing through one of the cables is very much greater than the field produced on the axis passing through a point midway between two of the cables. Using the results for the latter axis and assuming that the minimum value of the magnetic field that can be measured is 10^{-1} pT, we find that for a 100 Hz, 1000 A current in the cables the magnetic field can be measured up to h = 200 m away from the array, and for 1 Hz, 1000 A current in the cables the magnetic field can be measured up to h = 1 km away from the array.

The above field strength considerations are perhaps the most important in evaluating the possible undersea communication performance of cable array. However, there are a few other considerations that are also important, which we list before concluding this appendix. First, because communication is to take place from the bottom upwards in the sea, it may not be necessary for measurable electric or magnetic fields to be produced at the surface. Second, because most and perhaps all natural ULF/ELF noise in the sea comes from sources above the surface, the signal-to-noise ratio for communications via undersea cable arrays should increase with depth. Further, because the electric and magnetic

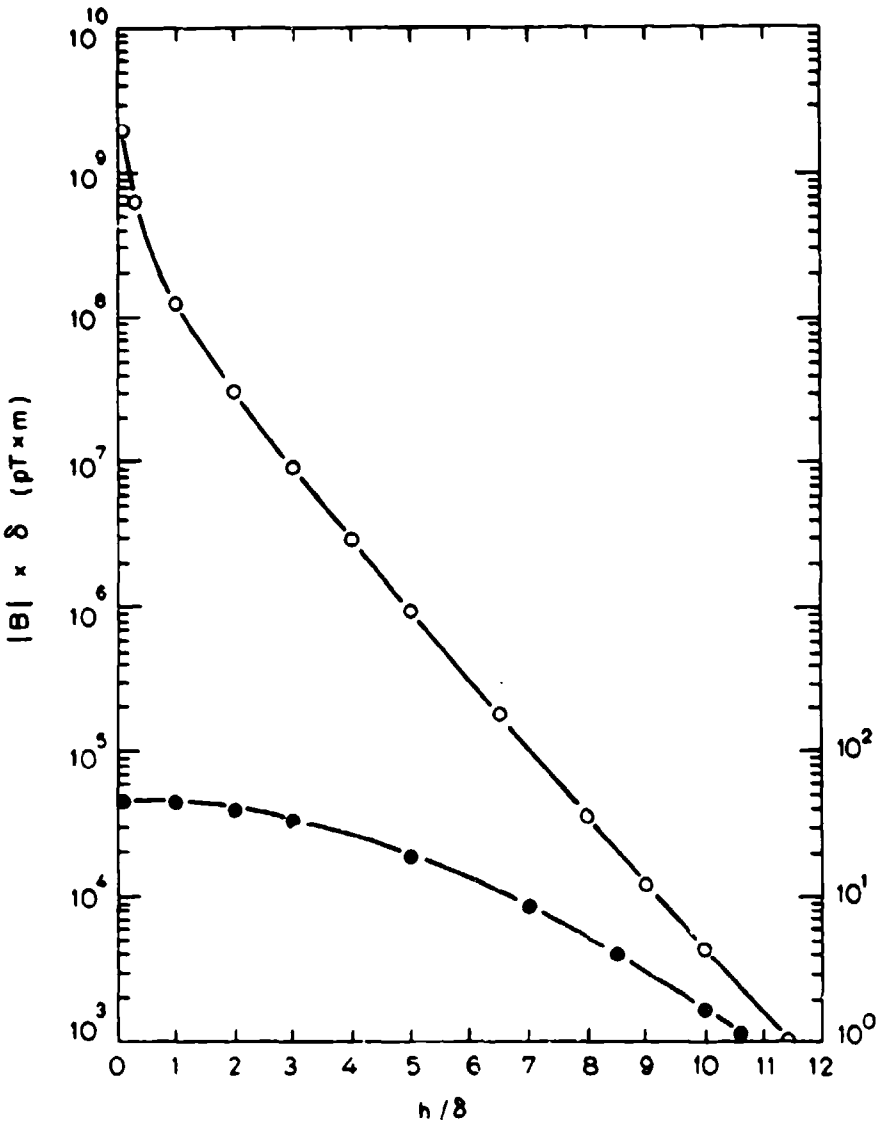

Figure D.3. Variation with perpendicular distance h (measured in skin depths δ) of the amplitude of the total magnetic field produced in a conducting medium above the plane of the series array shown in Figs. D.1(a) and D.2(a). It is assumed that the cables in the array carry a 1000 A alternating current and that they are spaced 30δ apart. The top curve (circles; left hand scale) shows the magnetic field produced along an axis perpendicular to the plane of the array and passing through one of the cables; the bottom curve (crossed circles; right hand scale) shows the magnetic field produced along an axis perpendicular to the plane of the array and passing through a point located midway between any two of the cables. The magnetic field direction for the top curve is along the x-axis, i.e., parallel to the plane of the array and perpendicular to the direction of the cables, and for the bottom curve the magnetic field direction is along the z-axis, i.e., perpendicular to the plane of the array.

fields from these natural sources are predominantly horizontally directed in the sea, it may be possible to discriminate against the natural noise by generating and measuring vertically-directed fields in the sea.

DISTRIBUTION LIST

Organization	No. of Copies
Director Defense Advanced Research Projects Agency	
ATTN: Program Management	2
TTO, R. A. Gustafson	1
TTO, P. A. Selwyn	1
1400 Wilson Boulevard Arlington, VA 22209	
Defense Technical Information Center Cameron Station Alexandria, VA 22314	12
Office of Naval Research	
ATTN: Code 414	1
Code 222	1
Code 425	1
800 North Quincy Street Arlington, VA 22217	
Office of Naval Research Resident Representative University of California, San Diego La Jolla, CA 92093	1
Office of Naval Research Resident Representative Stanford University Room 165 - Durand Building Stanford, CA 94305	1
Deputy Assistant Secretary of Defense Defense Research and Engineering for C^3	
ATTN: T. P. Quinn	1
Pentagon Washington, D.C. 20301	
Office of Assistant Secretary of the Navy (R, E&S)	
ATTN: J. Hull	1
Pentagon, Room 5E 779 Washington, D.C. 20350	

Organization	No. of Copies
Naval Research Laboratory Information Technology Division	
ATTN: J. R. Davis	1
4555 Overlook Avenue, SW Washington, D.C. 20375	
Naval Ocean Systems Center	
ATTN: Library	1
W. Moler	1
C. F. Ramstedt	1
Y. Richter	1
K. L. Grauer	1
271 Catalina Boulevard San Diego, CA 95152	
Naval Electronic Systems Command	
ATTN: PME-110-112	1
PME-110-X1	1
Department of the Navy Washington, D.C. 20360	
Naval Underwater Systems Center New London Laboratory	
ATTN: P. Bannister	1
A. Bruno	1
J. Orr	1
E. Soderberg	1
New London, CT 06320	
Naval Surface Weapons Center White Oak Laboratory	
ATTN: J. J. Holmes	1
M. B. Kraichman	1
P. Wessel	1
Silver Spring, MD 20910	
David W. Taylor Naval Ship Research and Development Center	
ATTN: W. Andahazy	1
F. E. Baker	1
P. Field	1
Annapolis, MD 21402	

DISTRIBUTION LIST (Continued)

Organization	No. of Copies
Naval Ocean R&D Activity	
ATTN: D. L. Durham	1
D. W. Handschumacher	1
K. Smits	1
NSTL Station	
Bay St. Louis, MS 39522	
Naval Oceanographic Office	
ATTN: O. E. Avery	1
T. Davis	1
G. R. Lorentzen	1
NSTL Station	
Bay St. Louis, MS 39522	
Naval Air Systems Command	
ATTN: B. L. Dillon	1
Washington, D.C. 20361	
Naval Intelligence Support Center	
ATTN: G. D. Batts	1
4301 Suitland Road	
Washington, D.C. 20390	
Naval Postgraduate School	
Department of Physics and Chemistry	
ATTN: O. Heinz	1
P. Moose	1
Monterey, CA 93940	
Naval Coastal Systems Center	
ATTN: R. H. Clark	1
M. J. Wynn	1
Panama City, FL 32407	
SRI International	
ATTN: D. M. Bubenik	1
J. B. Chown	1
R. C. Honey	1
333 Ravenswood Avenue	
Menlo Park, CA 94025	

Organization	No. of Copies
Science Application, Inc.	
ATTN: J. Czika, Jr.	1
1710 Goodridge Drive	
McLean, VA 22102	
Director	
Defense Nuclear Agency	
ATGTN: RAAE	2
DDST	1
RAEV	2
Washington, D. C. 20305	
R&D Associates	
ATTN: C. Greifinger	1
P. O. Box 9695	
Marina del Rey, CA 90291	
Pacific-Sierra Research Corp.	
ATTN: E. C. Field	1
1456 Cloverfield Boulevard	
Santa Monica, CA 90404	
Johns Hopkins University Applied Physics Laboratory	
ATTN: L. W. Hart	1
H. Ko	1
Johns Hopkins Road	
Laurel, MD 20810	
University of California Scripps Institute of Oceanography	
ATTN: C. S. Cox, Code A-030	1
La Jolla, CA 92093	
Lockheed Palo Alto Research Laboratory	
ATTN: W. Imhof	1
R. G. Johnson	1
J. B. Reagan	1
M. Walt	1
3521 Hanover Street	
Palo Alto, CA	

DISTRIBUTION LIST (Continued)

Organization	No. of Copies
La Jolla Institute ATTN: K. Watson La Jolla, CA 92407	1
University of Texas, Austin Geomagnetics and Electrical Geoscience Laboratory ATTN: F. X. Bostick, Jr. Austin, TX 78712	1
EG & G ATTN: L. E. Pitts P. O. Box 398 Riverdale, MD 20840	1
Chief Air Force Technical Applications Center HQUSAF Patrick AFB, FL 32925	1
Commander Air Force Systems Command Andrews AFB, MD 20331	2
Commander Air Force Geophysics Lab ATTN: Technical Library Hanscom AFB, MA 01731	1